

# Response to reviewers

Dear Editor, Dear Reviewers,

Thank you for considering our manuscript for publication in Geoscientific Model Development. Below, we address in detail each point raised by the reviewers, and describe the changes we have made to the manuscript in response to those points. In addition, we have made a few other changes, the most important being an added sentence in the abstract, and a reference to our simulation code, of which we have created a permanently available version with a DOI from zenodo. All the changes are visible in the marked-up manuscript provided further down in this pdf.

## Reviewer 1

Thank you for your comments. We are glad you agree with the motivation for the manuscript, and that you say it would be a welcome addition to the field. Regarding your comments, we address these below, and we also outline the changes we suggest to make in the manuscript.

### Major comments

#### Comment 1

The authors make the case for higher-order spatial interpolation, as if that is always better. However, there is no discussion at all about how the order of spatial interpolation is related to the order of the advection schemes within the OGCM from which the data is derived. Intuitively, I'd say that the most appropriate interpolation would be the scheme that most closely mimics the model advection scheme. I'd suggest the authors discuss this.

There are two points in this comment that we would like to address. First, it is not our intention to advocate higher-order interpolation as always better. There are advantages and disadvantages to all types of interpolation. Among the disadvantages of linear interpolation are the obviously unphysical discontinuous derivatives. Among the disadvantages of higher-degree splines is the increased computational effort per evaluation, and the possibility of overshoot/oscillations. The question we seek to address in this paper is of a numerical nature: "Given an interpolation scheme, which integrator gives the best balance between accuracy and performance?". We touch upon this in lines 333-335, but we agree that this can be made more clear in the manuscript. Towards the end of the introduction, around line 65 in the original manuscript, we have added the following:

"We note that the purpose of our investigation is not to determine how well different model resolutions and different interpolation schemes reproduce physical drifter trajectories. Rather, we address the purely numerical question of which combinations of integrator and interpolator give the best work-precision balance, for a given resolution."

Second, we feel that the point about using an advection scheme that mimics the ocean model is outside the scope of the paper. Our motivation is to provide guidance towards solving the common problem of integrating trajectories from offline velocity fields. Being a common oceanographic task, diverse ocean models are used, and each ocean model often has different advection schemes to choose from when configuring the model. For example, a popular ocean model, ROMS, offers four horizontal advection schemes for the user to choose from: second-order centered, fourth-order centered, fourth-order Akima and third-order upwind; e.g. see [https://www.myroms.org/wiki/Numerical\\_Solution\\_Technique#Horizontal\\_and\\_Vertical\\_Advection](https://www.myroms.org/wiki/Numerical_Solution_Technique#Horizontal_and_Vertical_Advection). Advection schemes in ocean modelling is also a topic of active research, and new methods are expected to be introduced. See for example

<https://www.sciencedirect.com/science/article/abs/pii/S146350031000106X>  
<https://www.sciencedirect.com/science/article/abs/pii/S1463500311001831>  
<https://www.sciencedirect.com/science/article/abs/pii/S1463500308001510>  
<https://archimer.ifremer.fr/doc/00435/54690/>

Additionally, information about the advection scheme is not always readily available for public ocean current data sets. It is therefore impractical to try to mimic an advection scheme for the general problem of interest studied here. Our intent is to help oceanographers implement an efficient method to integrate any ocean model velocity provided on a rectangular grid, without further concern.

#### **Comment 2**

The authors also but then quickly step over the problem of interpolation near land. Higher-order interpolation would mean that the halo of land is further extended into the ocean (as very briefly mentioned in line 362). I feel that this should be given more discussion. How would this problem compare to the error that the 'consistency of order  $p$  of the numerical method is no longer satisfied when the derivatives are not continuous' (lines 222-223)

It is worth commenting on this issue, but a full discussion would, we feel, be outside the scope of the current study. The global integration error is a universal issue that occur in all Lagrangian models using numerical integration of ODEs, while the handling of land is very much application dependent. For applications like LCS calculations, and global or large-scale transport simulations, interaction with the coastline may be almost negligible, whereas for applications like near-shore oil spills coastline interaction may be very important, and is implemented differently in different oil spill models (see, e.g., <https://www.mdpi.com/2077-1312/6/3/104>). Hence, it is impossible to say something generally applicable about how the error due to the handling of land cells compares to the global interpolation error.

We have added the following at line 364 in the original manuscript:

"Note that with higher-degree interpolation schemes, the fact that we set the currents to zero in land cells will have an effect on one or more of the closest cells to the coastline. For applications such as oil spill modelling, where shoreline interactions are important, a different strategy might be needed."

#### **Comment 3**

There is no discussion at all about the widely-used Analytical advection scheme of e.g. <https://doi.org/10.5194/gmd-10-1733-2017>. How does that scheme compare to the integrators discussed here?

Implementing a Lagrangian particle tracker with an interpolation scheme and an ODE solver can be accomplished very quickly, with just a few tens of lines of code in, e.g., Python or Matlab. As evidenced by the literature, many authors implement their own Lagrangian particle tracking codes in this way, and use different combinations of interpolation and integration schemes. Hence, we feel that the current manuscript provides useful information to the community, even without a detailed discussion/comparison to more advanced schemes.

While we are not very familiar with the advection scheme used in TRACMASS, it is our understanding that it (bi- or tri-) linearly interpolates the current internally in each cell based on vector components at the cell faces, and then solves analytically to find the passage of a particle through the interpolated field inside a cell. Rather than using a specified timestep or tolerance, this approach analytically calculates the trajectory through a cell as one step.

In the case of trilinear interpolation, it should be possible to compare our trajectories to those obtained with TRACMASS, but for the higher-degree interpolation schemes a direct comparison would be (numerically) meaningless. In any case, we feel that a detailed discussion/comparison to the TRACMASS trajectory scheme would be outside the scope of the current investigation, but might be an interesting topic for a future study.

#### **Comment 4**

The authors mention that they ignore diffusion (line 74). However, in most applications diffusion will be included in the computations. I wonder whether the errors caused by the

finite-sized set in the Wiener process are not much larger than any errors in interpolation as discussed here. It would be good if the authors could comment on this.

There are two points we would like to raise, in response to this comment. First a point on applications, and second an numerical/theoretical point.

First, although it is true that the addition of diffusion is common in many applications, there are also many oceanographic and atmospheric studies which will want to compute trajectories without diffusion. One example includes all LCS computations, as a requirement for LCS theory to hold is that the velocity be deterministic.

Furthermore, there are studies that deal with Lagrangian trajectories that intentionally do not include diffusivity. Examples include using backwards trajectories to investigate the source of particles that end up in the sediments in a particular location, and using Lagrangian trajectories to study the path and history of water arriving at a particular location of upwelling:

[www.nature.com/articles/ncomms7521](http://www.nature.com/articles/ncomms7521)

[journals.ametsoc.org/jpo/article/41/1/88/11315/A-Numerical-Modeling-Study-of-the-Upwelling-Source](http://journals.ametsoc.org/jpo/article/41/1/88/11315/A-Numerical-Modeling-Study-of-the-Upwelling-Source)

Second, the issue of adding diffusion is not entirely straightforward theoretically and numerically. Strictly speaking, advection-diffusion problems are not modelled with ODE methods, but with SDE methods, which are usually of lower order. While it might be common in practice to use a higher-order ODE method, and tack on a random displacement in an *ad hoc* manner, such a splitting of the problem is in itself an approximation which introduces an error. For spatially varying diffusivity, the short timestep required for the SDE method to give a sufficiently small error (in the weak sense) may also render the advection error irrelevant. A thorough discussion of this issue is definitely outside the scope of the paper.

However, it is of course clear that adding random increments to the position of a particle may in many cases dominate the numerical integration errors. In these cases, it would probably give little or no extra benefit to use higher-order integration schemes. To address this issue a bit more, we have added a subsection in the discussion, with the following two paragraphs (Section 5.3 in the revised manuscript):

“As mentioned in Section 2, we have considered pure advection, ignoring diffusion. Calculating trajectories with pure advection by a deterministic velocity field is common in several applications, perhaps most notably for identification of LCS (see, e.g., Haller (2015), Allshouse et al. (2017), Duran et al. (2018)). Other examples include the use of backwards trajectories to identify source regions for particles ending up in the sediments (van Sebille et al., (2015), and analysis of Lagrangian pathways to study the source and history of water parcels reaching a particular upwelling zone (Rivas & Samelson, 2011). In general, simulating diffusion in Lagrangian oceanography (or meteorology) may introduce a complication that encourages some studies to compute trajectories without diffusion: Lagrangian motion becomes ambiguous when diffusive mixing is simulated, because the identity of a fluid parcel is lost. On the other hand, ignoring small-scale mixing may also be problematic. One approach to this problem is to supplement purely advective trajectories with along-path changes in parcel properties, as discussed in Rivas & Samelson (2011).

However, for many other applications diffusion must be included. Solving the advection-diffusion equation with a particle method amounts to numerical solution of a stochastic differential equation (SDE), instead of an ODE. A range of different SDE schemes exist, and the details differ, but all such schemes involve adding a random increment at each timestep. If the random increment is far larger than the local numerical error in each step, then the numerical error in the advection is probably of limited practical importance. The details will depend on the application, and we encourage experimentation. A detailed description of numerical SDE schemes is outside the scope of this study, but the interested reader may find it useful to refer to, e.g., Kloeden & Platen (1992), Spivakovskaya et al. (2007), and Gräwe (2011).”

## Comment 5

I wonder why the authors don't test their method on (complex) flows where an exact solution is known. Quite a few of these flows have been used in the literature, including e.g. the Bickley Jet. That would save them a lot of challenges in defining the 'exact' solution.

An important motivation for avoiding an analytical reference solution, is that it seems likely that fifth-degree spline interpolation would out-perform cubic splines and linear interpolation in terms of accuracy, when comparing to an analytical solution. That would lead to the conclusion that higher-degree splines

give more accurate results, which is by no means certain for ocean currents. By using numerically obtained reference solutions, obtained separately for each interpolation scheme, we remain "interpolation-agnostic", merely addressing the question of which integrator/interpolator pair is numerically more efficient.

As mentioned in our response to comment 1, our intent is to help oceanographers implement an efficient method to integrate any ocean model velocity. Hence, we wanted the discussion and conclusions to feel directly relevant to applied oceanographers. For example, we conclude that the most efficient numerical approach for a given level of accuracy depends on the spatial resolution of the dataset. If we were to start with an analytically defined flowfield, and then discretely evaluate this on different grids, for later interpolation, it is not obvious how any conclusions could be applied directly to ocean current datasets.

#### **Comment 6**

I am not sure if comparing ends points is the most appropriate metric. Why not compare the along-trajectory differences, which is commonly used in the field (e.g. <https://doi.org/10.1029/2018JC014813>), so that the full trajectories are taken into account.

The endpoints were chosen simply because of the discussion in terms of the theory for numerical solution of ODEs. The standard approach in the ODE literature is to discuss convergence in terms of the global error, the order of a method refers to the global error, etc. In Figure 4, the error as a function of number of evaluations for the fixed-step integrators make straight lines in the log-log plot, with a slope determined by the order of convergence. If we considered the along-trajectory error, there would be less of a direct link to the theory of ODE methods when discussing these results.

From an application point of view, different metrics could be appropriate. For, e.g, LCS applications, only the endpoint matters, while for other applications the entire particle history might be relevant. In light of these points, we feel that the end points are, on the whole, the most appropriate metric.

#### **Comment 7**

The authors spend a large amount of attention on their 'special-purpose integrators' (section 3.3). However, they don't mention that most implementations of Lagrangian integrators would quite naturally implement such special-purpose integrators, simply because they don't store all time slices in memory so that they need to stop integration on the time of each time slice in order to load the next one.

We believe this is a misunderstanding by the reviewer. Taking the example of cubic interpolation, one needs at least 4 time slices in memory simultaneously to construct the interpolation. In the case of our special-purpose integrators, integration is stopped and restarted at every one of those time slices, not just when new data must be loaded.

For linear interpolation, two time slices will suffice to construct the interpolator, but in for example Taylor and Shadden (2008), which uses linear basis function interpolation and a variable-step Runge-Kutta-Fehlberg method, there is no description of stopping and restarting integration at every time slice. In our opinion, it is often hard to be sure of the exact details of how the full trajectory calculation has been implemented, given the typically very short descriptions of interpolation and integration schemes in the applied literature. Hence, a thorough discussion should be of value to the community, even if the method itself were to have been used by others before.

For fixed-step integrators, we do discuss the fact that these perform very well when the timestep is chosen such that integration is stopped and restarted at every time slice. See, e.g., lines 415–420 in the Discussion, and 515–520 in the Conclusion.

#### **Minor comments**

- line 4: clarify here that this is interpolation in space and time?

OK.

- line 16: 'computations on data from atmospheric models'?

OK.

- line 30: 'For all these applications'?

OK.

- line 36: 'capable' is an anthropomorphism; hyperbolic points are not capable of anything.

We have rephrased this to "... presenting hyperbolic points where initially small errors may grow exponentially."

- line 36: By whom is this recommended?

We have rephrased to "It may therefore be useful to employ higher-order integration methods ...".

- lines 43-54 and 126: It might be very useful to include a table with details of the different integrators, so that readers don't need to dig into the literature themselves to find out what the specifics are of each of these

This comment refers to the introduction, where we mention different integrators used in the applied literature. Given that these include not only Runge-Kutta methods, but also linear multistep methods and predictor-corrector methods, a useful description of these would probably require several pages. We don't see that a table could contain enough information to be useful, and for anyone who wants to implement these methods, looking them up would not be a large amount of work.

- line 55: 'very common' is perhaps too strong? Lagrangian oceanography is still a bit of a niche

We have removed "very".

- line 93: why is  $x$  not bold here?

We have left  $x$  in non-bold for the general theory discussion. We have added a brief explanation to make this more clear:

"In the following, we introduce some elements from the theory of numerical integration of ODEs, which will be needed for the later discussion. While elsewhere in this paper, we consider  $\mathbf{x}(t)$  as a two-dimensional vector giving the position of a particle in a horizontal plane, we here simply use  $x(t)$ , as the theory is general and can be applied to vectors and scalars alike."

- line 104 and other places: Would errors  $e$  and  $E$  not always be absolute values?

No. The error itself can be either positive or negative (see, e.g., Eq. (3.1) in Hairer et al. (1993)). However, when we discuss how the error scales with the timestep, it's the absolute value.

- line 172: At least summarise where these values 2.5 and 0.8 come from

Here there are two mistakes on our part, as the reference given doesn't actually discuss the choice in detail, and the parameters used in the code were actually 0.9 and 3.0. We have rephrased line 172 as follows:

"The factors 0.9 and 3.0 were chosen from a range of values recommended by Hairer et al. (1993, p. 168), and were kept constant for all numerical experiments."

- line 176: How does this extent to staggered grids (e.g. Arakawa-C) which are often used in oceanography?

Simply interpolate each vector component on its own grid. The vector components are interpolated separately, so this would require only a minimal change at the initialisation of the interpolators in our implementation.

- line 191: The word 'quite' is somewhat vague here

OK, will drop the word "quite".

- line 224: give some examples relevant to Lagrangian oceanography of these cases?

We have added the following at the end of line 225:

"The more pathological examples are perhaps unlikely to occur in practice. However, as we will see later, when the error in even a single step is unbounded by Eq. (7), this can in some cases dominate the global error, rendering the use of a higher-order scheme pointless."

- Figure 1: Also show (some of) the trajectories here, to give readers a feeling for the extent of dispersion?

We assume this comment is meant to refer to Figure 3? We have created a figure showing the final positions of the particles, for the three different datasets, which has been added as Fig. 4 in the revised manuscript.

- line 320: it is unclear at what depth the particles are released, and also whether they are advected in 2D or in 3D

OK. It is stated in line 360 of the original manuscript that we use only the surface layer of the currents, but we agree that this should be clearly described early in Section 4 as well. We have added the following at the end of the first paragraph of Section 4:

"We have chosen to consider two-dimensional (horizontal) transport only, using the surface layer of the modelled current data. The current velocity field is interpolated in three dimensions (two spatial dimensions plus time), using the same degree of interpolation in all three dimensions."

- line 329: is 'transport' the best word here?

We have changed this to "trajectories".

- line 363: explain what kind of padding is done

Padding was probably not the right word. It only means that when cropping the dataset, the subset selected was larger than the minimal size required to cover all the trajectories. We have rephrased this.

- line 373: explain why this creates additional discontinuities

This is somewhat technical, and hard to explain without going into details on how spline interpolations are constructed, which we have not covered in the paper. It is also a bit on the side, as we don't investigate this type of interpolator. Therefore, we would prefer not to go into detail, and simply refer the interested reader to Lekien and Marsden.

- line 381: what is the standard deviation/variability around this median? Are the differences between the runs larger than the variability within the runs?

We have created a new figure, added as Fig. B1 in the revised manuscript, where we show the range covering 90% of the errors. As this makes the figure somewhat more cluttered, we feel it is best to keep the original figure as it is, and add this new figure as a full-page figure in the Appendix. A reference to this new figure has been added in the first paragraph of Section 5.

- line 388, 389 and 390: even though the authors make a good point about comparing number of computations instead of runtime, here they still mention that runs are 'longer' and report runtime in seconds.

That is only meant to illustrate that each evaluation takes longer when higher-degree interpolation is used. However, in response to a comment by Reviewer 2, we have added an additional figure in the appendix showing error as a function of runtime, and we have expanded and rephrased the second paragraph of Section 5 as follows:

"Number of evaluations of the right-hand side was chosen as a measure of work, as it is more objective than the runtime of the simulation, which would depend on the particular machine used to run the simulations, and also be more susceptible to somewhat random variations. However, for the interested reader we show the error as a function of runtime in Fig. B2.

While we analyse the results in terms of number of function calls, we note that higher-order interpolation is more computationally costly than lower-order interpolation. This means that the same number of evaluations will take more time if a higher degree of interpolation is used. We found that for the simulations done with the fixed-step 4th-order Runge-Kutta integrator, the simulations with cubic spline interpolation took on average four to five times longer than those with linear interpolation, and the simulations with quintic spline interpolation took on average three to four times longer than those with cubic spline interpolation."

- Figure 4: I'm a bit confused by the number of points on each of these lines. Why do some have 11 points, even though according to table 1 there were only 9 time steps and 10 tolerances tested?

This was an inconsistency between Table 1 and the figures, where we had included a tolerance of  $10^{-14}$  in the results, but forgotten to add it to Table 1. We have fixed this.

- Table 2: Would this data be easier to parse in a figure instead of a table?

In our opinion, a table is most suited in this case.

- line 493: mention what is 'special' about these special-purpose integrators (e.g. 'that don't step across time grids' or something like that)

We have rephrased the end of the second paragraph in Section 6 as follows:

"... This is achieved by stopping and restarting the integration exactly at the grid points of the dataset along the time dimension. By doing this, we avoid stepping across discontinuities in the (higher) derivatives of the velocity field, and we thus avoid picking up local errors that are unbounded by Eq. (7) at those points."

## Reviewer 2

Thank you for your encouraging comments. Below, we address the suggested changes to our manuscript.

### Major comments

#### Comment 1

Section 4.1: All three data sets have the same constant temporal resolution of 1 hour. Since one of the key advantages of the proposed time-varying integrators is to better treat temporal discontinuities in the sampled flow field, I'm wondering if varying temporal resolutions might have an impact on the analysis as well? Some clarification, either in section 4 or 5 would help here, or possibly even an additional test case with a known analytical solution and different temporal resolutions could be used to highlight this (something akin to 3.2, but comparing fixed / time-varying / special-purpose integrators).

There is some effect of temporal resolution. We did some tests initially, but these were not completed or included in the manuscript, as we felt it would be too long. We also re-ran some of those tests now (with the same datasets, but downsampled to 6 hours temporal resolution), and from a quick analysis, the results appear relatively similar to those presented here. The improvement seen for the special-purpose integrators appears a little smaller for datasets with coarser temporal resolution, but not by a large amount. The reason is the relative importance of crossing discontinuities in the time dimension relative to the spatial dimensions. This is discussed in lines 429-437 of the original manuscript, when discussing the different spatial resolutions.

While the effect of temporal resolution would be an interesting investigation for a future study, we have concluded that we would rather not include it in the current paper, mainly for reasons of length. Presenting the new results takes some space, new reference solutions must be established and documented, and the discussion would have to be expanded. We would also run into questions about resolving the tides, and in particular when the dataset with 800 m resolution is downsampled to 6 hours temporal resolution, the typical current velocities of about 0.25 m/s will move many cells during a timestep, meaning that the low temporal resolution might be inadequate to capture the dynamics of the high-resolution data. All in all, we feel that a thorough discussion of these issues would make the paper too bloated.

#### Comment 2

Section 4.4: "We used only the surface layer of the data sets", but then 3D spline interpolators are used. Are the experiments considering 2-dimensional trajectories or 3-dimensional ones? Please clarify.

Time is the third dimension used in the interpolator. This is mentioned in lines 368/369, but we will make this more clear earlier in section 4, in line with our reply to comments by Reviewer 1. We have added the following at the end of the first paragraph of Section 4:

”We have chosen to consider two-dimensional (horizontal) transport only, using the surface layer of the modelled current data. The current velocity field is interpolated in three dimensions (two spatial dimensions plus time), using the same degree of interpolation in all three dimensions.”

### Comment 3

Section 5.: ”Number of evaluations of the right-hand side was chosen as a measure of work, as it is more objective than the runtime of the simulation” is almost immediately followed by ”We note that higher-order interpolation is more computationally costly than lower order interpolation.” While both statements are correct in their own context, they seem a little contradictory here. A small clarification could help clarify this. Moreover, while I agree that the number of evaluations is an important metric to evaluate the efficiency of different numerical integrators, the overall time-to-solution is often the final metric in practice. The final paragraph of 5.2 hints at this, but I’m left wondering if a graph plotting error vs. run-time could be used to highlight the points here more clearly?

We have added an additional figure in the appendix showing error as a function of runtime, and we have expanded and rephrased the second paragraph of Section 5 as follows:

“Number of evaluations of the right-hand side was chosen as a measure of work, as it is more objective than the runtime of the simulation, which would depend on the particular machine used to run the simulations, and also be more susceptible to somewhat random variations. However, for the interested reader we show the error as a function of runtime in Fig. B2.

While we analyse the results in terms of number of function calls, we note that higher-order interpolation is more computationally costly than lower-order interpolation. This means that the same number of evaluations will take more time if a higher degree of interpolation is used. We found that for the simulations done with the fixed-step 4th-order Runge-Kutta integrator, the simulations with cubic spline interpolation took on average four to five times longer than those with linear interpolation, and the simulations with quintic spline interpolation took on average three to four times longer than those with cubic spline interpolation.”

### Comment 4

Section 6: ”The most striking conclusion from the results presented above.” This reads more like a continuation of the discussion above, rather than a conclusion in its own right. Maybe re-structure a little to independently re-state the objective and key findings of the paper, as is to some extent done later in the section?

We have expanded and rephrased the start of Section 6 as follows:

“In this paper, we have investigated how different numerical integrators behave, in combination with different degrees of interpolation, and datasets of different spatial resolution. We have calculated trajectories over 72 hours, from 10000 initial positions, and compared the integrator-interpolator pairs in terms of the error in the final position of each trajectory. We have considered linear, cubic and quintic spline interpolation, along with four fixed-step Runge-Kutta integrators of orders 1 to 4, three commonly used variable-step integrators, and three special-purpose variants of the latter.

The most striking conclusion from our results is that the special-purpose integrators we describe in many cases deliver several orders of magnitude more accurate results, at no additional cost. Alternatively, they can deliver the same accuracy as standard methods, with highly reduced computational effort. This is achieved by stopping and restarting the integration exactly at the grid points of the dataset along the time dimension. By doing this, we avoid stepping across discontinuities in the (higher) derivatives of the velocity field, and thus we avoid picking up local errors that are unbounded by Eq. (7) at those points.”

## Minor comments

\* Link to data sets strictly requires ‘https://’ in the URL. Please adjust footnote on p.12.

This has been fixed.



\* The code repository on github is very neat (much appreciated!), but I could not find the Jupyter notebooks mentioned in the text. (In case I just missed them, maybe a link in the README in the repo would help people find them quickly?)

The notebooks were indeed missing. Our apologies. We have added the notebooks to the repo, and created a “release” with a DOI that can be cited.

# Numerical integrators for Lagrangian oceanography

Tor Nordam<sup>1,2</sup> and Rodrigo Duran<sup>3,4</sup>

<sup>1</sup>SINTEF Ocean, Trondheim, Norway

<sup>2</sup>Department of Physics, Norwegian University of Science and Technology, Trondheim, Norway

<sup>3</sup>National Energy Technology Laboratory, Albany, OR 97321, USA

<sup>4</sup>Theiss Research, San Diego, CA 92037, USA

**Correspondence:** Tor Nordam (tor.nordam@sintef.no)

**Abstract.** A common task in Lagrangian oceanography is to calculate a large number of drifter trajectories from a velocity field pre-calculated with an ocean model. Mathematically, this is simply numerical integration of an Ordinary Differential Equation (ODE), for which a wide range of different methods exist. However, the discrete nature of the modelled ocean currents requires interpolation of the velocity field [in both space and time](#), and the choice of interpolation scheme has implications for the accuracy and efficiency of the different numerical ODE methods.

We investigate trajectory calculation in modelled ocean currents with 800 m, 4 km, and 20 km horizontal resolution, in combination with linear, cubic and quintic spline interpolation. We use fixed-step Runge-Kutta integrators of orders 1–4, as well as three variable-step Runge-Kutta methods (Bogacki-Shampine 3(2), Dormand-Prince 5(4) and 8(7)). Additionally, we design and test modified special-purpose variants of the three variable-step integrators, that are better able to handle discontinuous derivatives in an interpolated velocity field.

Our results show that the optimal choice of ODE integrator depends on the resolution of the ocean model, the degree of interpolation, and the desired accuracy. For cubic interpolation, the commonly used Dormand-Prince 5(4) is rarely the most efficient choice. We find that in many cases, our special-purpose integrators can improve accuracy by many orders of magnitude over their standard counterparts, with no increase in computational effort. [Equivalently, the special-purpose integrators can provide the same accuracy as standard methods, at a reduced computational cost.](#) The best results are seen for coarser resolutions (4 km and 20 km), thus the special-purpose integrators are particularly advantageous for research using regional to global ocean models to compute large numbers of trajectories. Our results are also applicable to trajectory computations [on data](#) from atmospheric models.

*Copyright statement.* TEXT

## 20 1 Introduction

Calculating trajectories of tracers through a pre-calculated velocity field is a common task for many applications (van Sebille et al., 2018). Oceanic and atmospheric transport simulations are frequently built on this approach, and used to calculate, for

example, the transport of pollutants (see, e.g., Rye et al. (1998); North et al. (2011); Povinec et al. (2013); Onink et al. (2019)), distribution of algae and plankton (see, e.g., Siegel et al. (2003); Woods (2005); Visser (2008)), search and rescue operations (see, e.g., Breivik and Allen (2008); Serra et al. (2019)), or temperature and salinity pathways (see, e.g., Barkan et al. (2017)). Similarly, climate change studies may compute vast numbers of trajectories to understand transport of heat and salt (see, e.g., Dugstad et al. (2019)). Computation of trajectories for a variety of atmospheric species are also a common application (see, e.g., Sirois and Bottenheim (1995); Riuttanen et al. (2013); Nieto and Gimeno (2019)). Other applications include the calculation of Lagrangian Coherent Structures (LCS), which is not a transport simulation *per se*, but which still uses tracer trajectories to analyze flow fields (see, e.g., Farazmand and Haller (2012); Onu et al. (2015); Haller (2015); Duran et al. (2018)).

For all of these applications, it is of interest to obtain trajectories of the desired accuracy with minimal computational work, or conversely, to obtain the most accurate solution possible for a given amount of computational effort. Marine and atmospheric transport applications often require computing large numbers of trajectories, which are essentially solutions of an ordinary differential equation (ODE). As this can be computationally quite demanding, guidance on how to select the optimal combination of numerical schemes for a given application is of practical value.

We further note that in ODE parlance, the velocity fields represented by ocean currents (and wind) may be both stable and unstable, often presenting hyperbolic points ~~capable of exponentially growing where~~ initially small errors ~~. It is therefore recommended to use~~ may grow exponentially. It may therefore be useful to employ higher-order integration methods, or small time steps with lower-order integration methods. This is particularly relevant for long integration times (months to years) where error accumulates and can be amplified.

In the applied mathematics community, a standard first choice for numerically solving an ODE is a variable-step integrator (see, e.g., Gladwell et al. (2003)). Variable-step integrators use clever choices of function evaluations in order to evaluate the local error in each step of the solution, and the time-step is dynamically chosen to be as long as possible while meeting a prescribed error estimate. Thus, variable-step integrators tend to be more efficient than their fixed-step counterparts.

However, there is limited discussion of such an approach in the literature on applied Lagrangian oceanography. Integrators used in marine transport applications may range from Euler's method (see, e.g., Zelenke et al. (2012); De Dominicis et al. (2013)), to a more typical 4th-order Runge-Kutta method (see, e.g., García-Martínez and Flores-Tovar (1999)). Some alternatives seek to cut on computational time by using less evaluations, like the 4th-order Milne-predictor, Hamming-corrector integration scheme (see, e.g., Narváez et al. (2012)), or the 4th-order Adams-Bashforth method (see, e.g., Yang et al. (2008)).

In the context of LCS, variable-timestep integrators appear to be a more common, yet not universal, choice. Interpolation schemes, which must be used to evaluate discretely gridded velocity fields at arbitrary points, have also received some attention in the LCS field. Ali and Shah (2007) use a 4th-order Runge-Kutta-Fehlbergh method and the local cubic interpolation recipe of Lekien and Marsden (2005). Beron-Vera et al. (2008) use linear interpolation and the classic 4th-order Runge-Kutta. Shadden and Taylor (2008) use linear basis functions for interpolation, and a Runge-Kutta-Fehlberg scheme for integration. Peng and Dabiri (2009) use the 4th-order Runge-Kutta with a velocity field derived from Particle Image Velocimetry (PIV), though with no interpolation scheme specified.

Solving diverse types of marine-transport problems is ~~very common~~ a common task, and given the vast number of computations that are often involved, it seems natural to ask how variable-step integrators perform. Because a pre-calculated velocity field is necessarily given at discrete times and spatial locations, interpolation must be used to create continuous representations of these velocity fields that can then be integrated using numerical schemes. In practice, the choice of an interpolation scheme will have implications for the accuracy that can be achieved with the different numerical integrators, as well as the computational effort.

In this paper, we compare several approaches for interpolation of the velocity field, and numerical integration of the trajectories. We include both fixed and variable stepsize integrators. As input data to the trajectory calculations, we use modelled ocean currents at 20 km, 4 km and 800 m resolutions. These are representative of current high-resolution Earth Modeling Systems, regional (eddy-resolving) ocean models and submesoscale-resolving ocean models, respectively (Lévy et al., 2012), and thus span a wide range of applications.

We note that the purpose of our investigation is not to determine how well different model resolutions and different interpolation schemes reproduce physical drifter trajectories. Rather, we address the purely numerical question of which combinations of integrator and interpolator give the best work–precision balance, for a given resolution.

The layout of this paper is as follows: In Section 2, we introduce some theory on numerical integration of ODEs, including a description of the interpolation and integration schemes used, and a discussion of the local and global error of numerical integrators. Next, in Section 3 we discuss the performance of numerical integrators for velocity fields with discontinuous derivatives, and describe how we modified well-known variable-step integrators to improve their performance for this particular application. Section 4 describes how the interpolation and integration schemes were implemented in code, and the numerical experiments that were carried out. Section 5 contains the results of our investigation, and a discussion of the results, and finally in Section 6 we present some conclusions on the most efficient choice of integrator for different applications.

## 2 Theory

The topic of the current paper is to study the numerical calculation of tracer advection by precalculated, gridded velocity fields, with a focus on applications in Lagrangian oceanography. Note that we ignore diffusion, and consider pure advection with ocean currents. In this case, the trajectory of a particle being advected passively through a velocity field is defined by the ODE

$$\dot{\mathbf{x}} = \mathbf{v}(\mathbf{x}, t), \tag{1}$$

where  $\mathbf{v}(\mathbf{x}, t)$  is the velocity at position and time  $(\mathbf{x}, t)$ , along with an initial condition,  $\mathbf{x}(t_0) = \mathbf{x}_0$ . Such a problem is called an initial value problem, and solving it means to find the value of  $\mathbf{x}(t)$  at later times,  $t > t_0$ .

Finding the solution of an initial value problem by numerical means is known as numerical integration of the differential equation. A large body of literature exists on the topic of numerical integration, and a range of different techniques exist, both general-purpose methods that work with many different problems (see, e.g., Hairer et al. (1993); Hairer and Wanner (1996)), and special-purpose methods that for example preserve some symmetry of the problem (see, e.g., Hairer et al. (2006)). In this paper, we will consider both fixed- and variable-step methods from the Runge-Kutta family.

90 In the following, we introduce some elements from the theory of numerical integration of ODEs, which will be needed for the later discussion. While elsewhere in this paper, we consider  $\mathbf{x}(t)$  as a two-dimensional vector giving the position of a particle in a horizontal plane, we here use simply  $x(t)$ , as the theory is general and can be applied to vectors and scalars alike.

Common to all numerical ODE methods is that they make discrete steps in time. In a fixed-step method, time is incremented by a fixed amount,  $h$ , at each iteration, and we have

95  $t_n = t_0 + nh.$  (2)

For the variable-step methods, the value of the timestep may change throughout the simulation, such that  $t_n + h_n = t_{n+1}$ . Hence, the relationship between time and timestep in this case becomes

$$t_n = t_0 + \sum_{i=0}^{n-1} h_i, \quad n \geq 1. \quad (3)$$

For both types of methods, if the solution is to be calculated up to time  $t_N$ , we adjust the last timestep as necessary to, stop the  
100 integration exactly at  $t_N$ :

$$h_{N-1} \rightarrow \min(h_{N-1}, t_N - t_{N-1}). \quad (4)$$

Finally, we will use notation where we let  $x_n$  denote the numerically obtained solution at time  $t_n$ , and we let  $x(t_n)$  be the *true* solution at time  $t_n$ . Note that while  $x(t_n)$  is usually not known, we will still assume that there exists a unique, true solution (Hairer et al., 1993, pp 35–43).

## 105 **2.1 Error Bounds**

Since numerical integration is most commonly used in situations where the exact solution is unknown, it becomes necessary to estimate the error by purely numerical means. In general, the idea is that a smaller timestep,  $h$ , gives a more accurate solution, and as  $h \rightarrow 0$ , the numerically obtained solution converges to the true solution. The rate of convergence depends on the chosen integration method.

110 There are two important measures of the error: The *local* error and the *global* error. The local error is the error made in a single step. Assume there is no error in the position at time  $t_{n-1}$ , that is,  $x(t_{n-1}) = x_{n-1}$ . Then, the local error in step  $n$  is given by (Hairer et al., 1993, p. 156)

$$e(h) = x(t_n) - x_n. \quad (5)$$

The global error, on the other hand, is the error at the end of the computation, at time  $t_N$  (assuming  $x(t_0) = x_0$ ), and is given  
115 by (Hairer et al., 1993, p. 159)

$$E(h) = x(t_N) - x_N. \quad (6)$$

It can be shown that for a Runge-Kutta method of order  $p$ , and for an ODE given by  $\dot{x} = f(x, t)$ , where all partial derivatives of  $f(x, t)$  up to order  $p$  exist and are continuous (that is,  $f \in C^p$ ), the local error is bounded by

$$|x(t_0 + h) - x_1| \leq Ch^{p+1}, \tag{7}$$

120 where  $C$  is some constant, which depends on the method and on the partial derivatives of  $f(x, t)$  (Hairer et al., 1993, p. 157). If the local error is  $\mathcal{O}(h^{p+1})$ , then the global error will be  $\mathcal{O}(h^p)$  (Hairer et al., 1993, pp. 160–162). When the global error is proportional to  $h^p$ , the method is said to be of order  $p$ .

## 2.2 Numerical integration methods

We have chosen to consider seven different numerical integration schemes, all from the family of Runge-Kutta methods. These  
125 include four methods with fixed timestep:

- 1st-order Runge-Kutta (Euler’s method),
- 2nd-order Runge-Kutta (explicit trapezoid),
- 3rd-order Runge-Kutta (Kutta’s method),
- 4th-order Runge-Kutta,

130 For details of these methods, we refer to, e.g., Griffiths and Higham (2010, pp. 24, 44–45, and 131). We have also considered three methods with variable timestep:

- Bogacki-Shampine 3(2),
- Dormand-Prince 5(4),
- Dormand-Prince 8(7).

135 For further details of these methods, we refer to Bogacki and Shampine (1989), and Dormand and Prince (1980, 1986).

As an example, and to aid the explanation of the timestep adjustment routine which will follow in Sections 2.3 and 3.3, we will describe the Bogacki-Shampine 3(2) method in some detail. For an ODE given by

$$\dot{x} = f(x, t), \tag{8}$$

the Bogacki-Shampine 3(2) method, for making a step from position  $x_n$ , at time  $t_n$ , to position  $x_{n+1}$ , at time  $t_{n+1} = t_n + h_n$ ,  
 140 is

$$k_1 = f(x_n, t_n) \tag{9a}$$

$$k_2 = f(x_n + \frac{1}{2}k_1h_n, t + \frac{1}{2}h_n) \tag{9b}$$

$$k_3 = f(x_n + \frac{3}{4}k_2h_n, t + \frac{3}{4}h_n) \tag{9c}$$

$$k_4 = f(x_n + \frac{2}{9}k_1h_n + \frac{1}{3}k_2h_n + \frac{4}{9}k_3h_n, t + h_n) \tag{9d}$$

$$145 \quad \hat{x}_{n+1} = x_n + \frac{7}{24}k_1h_n + \frac{1}{4}k_2h_n + \frac{1}{3}k_3h_n + \frac{1}{8}k_4h_n \tag{9e}$$

$$x_{n+1} = x_n + \frac{2}{9}k_1h_n + \frac{1}{3}k_2h_n + \frac{4}{9}k_3h_n. \tag{9f}$$

This provides two estimates of the next position, of which  $x_{n+1}$  is of order 3, and  $\hat{x}_{n+1}$  is of order 2. For this method, the  
 higher order estimate is used to continue the integration (known as local extrapolation, see Hairer et al. (1993, p. 168)), while  
 the lower order estimate is used to calculate  $|x_{n+1} - \hat{x}_{n+1}|$ , which is used to estimate the local error and adjust the timestep  
 150 (see Section 2.3).

Comparing Eqs. (9d) and (9f), we note that  $k_4 = f(x_{n+1}, t_{n+1})$ . Hence, the weights of this method are chosen such that  $k_4$   
 at one step is equal to  $k_1$  at the next step. This property is known as First Same As Last (FSAL), and saves one evaluation of  
 the right-hand side for every step after the first (see, e.g., Hairer et al. (1993, p. 167)). Hence, with only three new evaluations  
 of  $f(x, t)$ , this method can provide both a third-order estimate used to continue the integration, and a second order estimate for  
 155 error control.

Dormand-Prince 5(4) uses 7 evaluations of  $f(x, t)$ , to construct a 5th-order estimate for continuing the integration, and a  
 4th-order estimate for error control and timestep adjustment. This method also has the FSAL property, meaning that it uses  
 only 6 evaluations for every step after the first. The final method considered, Dormand-Prince 8(7), uses 13 evaluations of  
 $f(x, t)$  to construct 8th-order and 7th-order estimates, of which the 8th-order is used to continue the integration. This integrator  
 160 does not have the FSAL property.

### 2.3 Timestep adjustment

In the code used to carry out numerical experiments, timestep adjustment has been implemented based on the description in  
 Hairer et al. (1993, pp. 167–168). The user must specify two tolerance parameters, the absolute tolerance,  $T_A$ , and the relative  
 tolerance,  $T_R$ . We then want the estimate of the local error to satisfy

$$165 \quad |x_{n+1} - \hat{x}_{n+1}| \leq T_A + T_R \cdot \max(x_n, x_{n+1}). \tag{10}$$

To provide a measure of the error, we introduce  $\bar{e}$ , which is a normalised numerical estimate of the true local error (Eq. (5)), given by

$$\bar{e} = \sqrt{\sum \left( \frac{x_{n+1} - \hat{x}_{n+1}}{T_A + T_R \cdot \max(|x_n|, |x_{n+1}|)} \right)^2}, \quad (11)$$

where in our case we take the sum over the two vector components of the solution. We would like to find the optimal timestep, in the sense of giving the optimal balance between error and computational speed. We consider this to be the timestep where the estimated local error is equal to error allowed by the tolerance, in which case we have  $\bar{e} = 1$ . If, after calculating  $\hat{x}_{n+1}$  and  $x_{n+1}$ , we find that  $\bar{e} \leq 1$ , the step is *accepted*, we update the time to  $t_{n+1} = t_n + h_n$ , and proceed with the calculation from the new position  $x_{n+1}$ . If, on the other hand,  $\bar{e} > 1$ , the step is *rejected*, and we remain at position  $x_n$ , and attempt to make the step again with a reduced timestep.

For both accepted and rejected steps, we adjust the timestep after every step. Since  $\bar{e}$  scales with  $h^{q+1}$ , where  $q$  is the lower order of the two estimates  $\hat{x}_{n+1}$  and  $x_{n+1}$ , we have that the optimal timestep,  $h_{\text{opt}}$ , is given by (Hairer et al., 1993, p. 168)

$$h_{\text{opt}} = h_n (1/\bar{e})^{\frac{1}{q+1}}. \quad (12)$$

A rejected step represents wasted computational work. Hence, in order to make it more likely that the next step is accepted, we set the timestep to a value somewhat smaller than  $h_{\text{opt}}$ , and we also seek to prevent the timestep from increasing too fast:

$$h_{n+1} = \min(2.5 \cdot h_n, 0.8 \cdot h_{\text{opt}}) \quad (13)$$

~~See Hairer et al. (1993, p. 168) for additional discussion of the choice of the factors 0.8 and 2.5~~ The factors 0.9 and 3.0 were chosen from a range of values recommended by Hairer et al. (1993, p. 168), and were kept constant for all numerical experiments. The same timestep adjustment routine, as described above, has been used for all three variable-timestep methods used in this paper.

## 2.4 Interpolation

Modelled ocean current velocity data used in Lagrangian oceanography are commonly provided as vector components given on regular grids of discrete points,  $(x_i, y_j, z_k)$ , as well as discrete times  $t_n$ . In order to calculate the trajectory of a particle that moves in the velocity field defined by these data, we will have to evaluate the vector field at arbitrary locations, and (for variable-step methods) arbitrary times. An important point for our purposes is that the local error of an order  $p$  Runge-Kutta method is only bounded by  $Ch^{p+1}$  if all partial derivatives up to order  $p$  of the velocity field,  $\mathbf{v}(\mathbf{x}, t)$  in Eq. (1), exist and are continuous. This has implications for how we should evaluate the gridded velocity field used in a particle transport simulation. For example, if one uses linear interpolation, the first partial derivatives will be constant inside a cell, but discontinuous at cell boundaries. Hence, even for a first-order method the local error is not guaranteed to be bounded by Eq. (7) when stepping across a cell boundary (either in space or time).

In this study, we have chosen to consider three different interpolation schemes, using the same order of interpolation in both space and time:



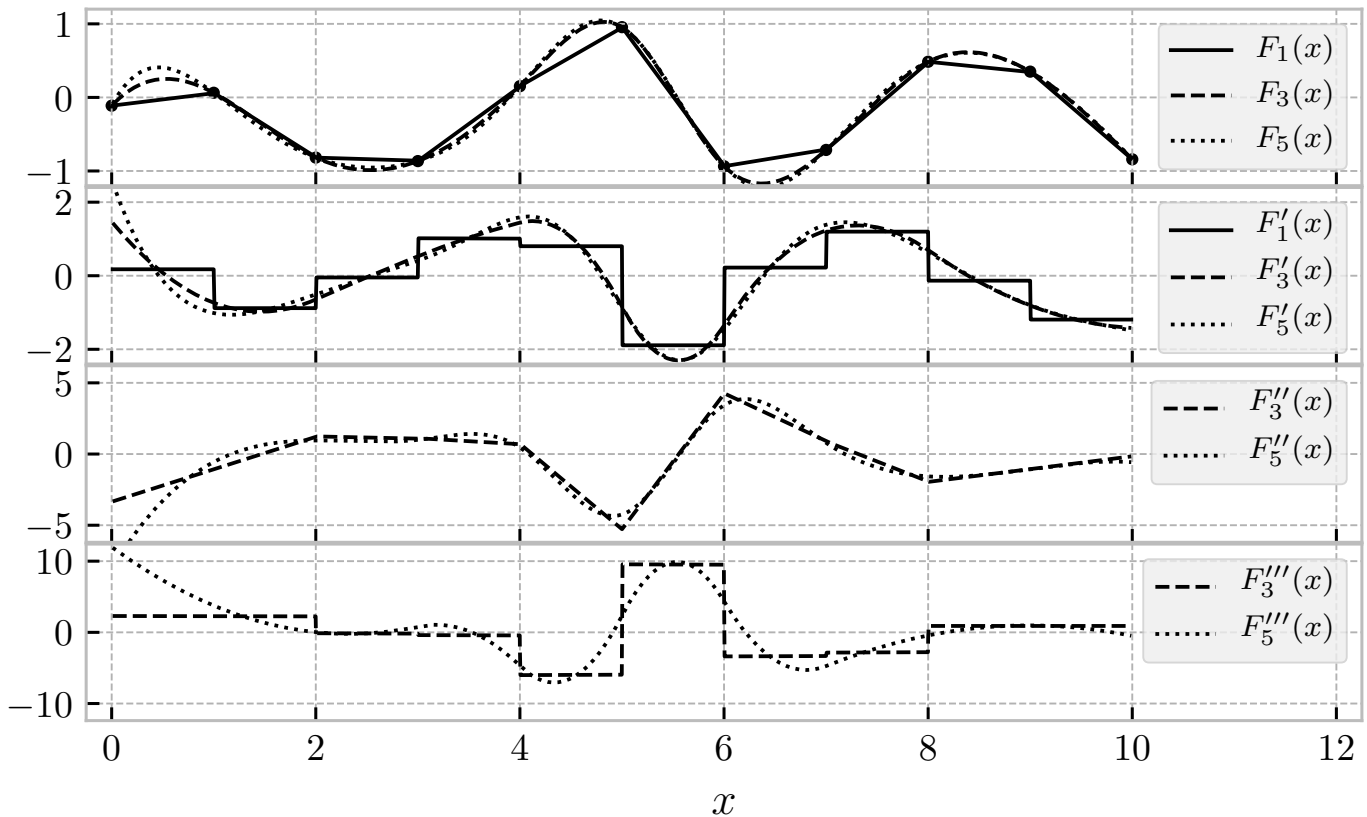


**Figure 1.** One-dimensional illustration of different degrees of interpolation. From the same 11 data points (shown as black circles in the top panel), we have constructed a linear interpolation (continuous lines), a cubic spline interpolation (dashed lines), and a quintic spline interpolation (dotted lines). From the top, the panels show the interpolated functions, the first derivative, the second derivative, and the third derivative. We observe that linear interpolation,  $F_1(x)$ , gives a discontinuous derivative, and cubic interpolation,  $F_3(x)$ , gives a discontinuous third derivative.

- Second order: Linear interpolation
- Fourth order: Cubic spline interpolation
- Sixth order: Quintic spline interpolation

200 Note that the order of interpolation is 1 plus the polynomial degree (de Boor, 2001, p. 1).

To aid the later discussion, we will briefly explain spline interpolation in one dimension. The generalisation to higher dimensions is quite natural. Assume that we have a grid of  $N$  equidistant points,  $x_n \in \{x_1, x_2, \dots, x_{N-1}, x_N\}$ , and the values of some function in those points,  $y_n = f(x_n)$ . The aim of an interpolation procedure is to allow us to approximate the function  $f(x)$  at arbitrary  $x$ , subject to  $x_1 \leq x \leq x_N$ . In the case of linear interpolation, the value of the linearly interpolated function,

205  $F_1(x)$  on the interval  $[x_n, x_{n+1}]$  is given by

$$F_1(x) = f(x_n) + \frac{x - x_n}{\Delta x} \cdot (f(x_{n+1}) - f(x_n)), \quad (14)$$

where  $\Delta x = x_{n+1} - x_n$  is the grid spacing. We see that  $F_1(x)$  is a continuous function, but its derivative,  $F_1'(x)$ , is not continuous at the grid points.

210 A cubic spline interpolation,  $F_3(x)$ , of the same data points as above will be given on an interval  $[x_n, x_{n+1}]$  by a cubic polynomial, e.g.,

$$F_3(x) = w_0 + w_1\tilde{x} + w_2\tilde{x}^2 + w_3\tilde{x}^3, \quad (15)$$

where  $\tilde{x} = x - x_n$ , and the weights,  $w_0, w_1, w_2$  and  $w_3$  are chosen such that  $F_3(x), F_3'(x)$ , and  $F_3''(x)$  are all continuous at the grid points (see, e.g., Press et al. (2007, pp. 120–124)). By the same token, a fifth-degree spline interpolation gives a piecewise polynomial function of degree 5, with the property that the first, second, third and fourth derivatives are continuous at the grid points. A one-dimensional illustration of the three degrees of interpolation considered in this paper is provided in Fig. 1. For a description of how spline interpolation of ocean current velocity fields was implemented, see Section 4.

220 Finally, we would like to note two important points on the subject of interpolation in Lagrangian oceanography. First, the purpose of interpolating discrete current data is *not* to approximate the unresolved turbulent motion of the ocean, but simply to provide a consistent recipe for evaluating gridded data at arbitrary locations. Second, once an interpolation scheme has been chosen, one has effectively replaced the gridded input data by a set of analytical expressions, specifying a way in which to evaluate the velocity field at any point and time. Hence, for a given dataset and interpolation scheme, the initial value problem given by  $\dot{\mathbf{x}} = \mathbf{v}(\mathbf{x}, t)$ ,  $\mathbf{x}(t_0) = \mathbf{x}_0$ , has a unique *true solution* (provided the usual conditions for existence and uniqueness of solutions of ODEs are met, see, e.g., Hairer et al. (1993, pp 35–43)). With increasingly short timestep,  $h \rightarrow 0$ , stable and consistent numerical integration schemes should converge towards the true solution. However, velocity fields evaluated with

225 *different* orders of interpolation are *not* identical, and will not produce identical trajectories, even as  $h \rightarrow 0$ .

### 3 Special-purpose integrators

In this section, we will discuss the implications of our ODE having a right-hand side with discontinuous derivatives. We consider an analytical example with one discontinuity to illustrate the problem, and present a modified, special-purpose integration routine that handles the discontinuity. We then describe how to implement the same idea in special-purpose variants of regular variable-step integrators, for application in Lagrangian oceanography.

230

#### 3.1 Discontinuous derivatives

As mentioned in Section 2.1, the conditions for a  $p$ th-order Runge-Kutta method to actually be  $p$ th-order accurate, require continuous derivatives of the right-hand side, up to and including order  $p$ . The problem is that consistency of order  $p$  of the numerical method is no longer satisfied when the derivatives are not continuous (Kress, 1998, pp. 235, 252). In many cases this

235 means that the error is larger than expected, but in some cases the problem may be more serious: the numerical approximation may be meaningless (Isaacson and Keller, 1994, p. 346). The more pathological examples are perhaps unlikely to occur in practice. However, as we will see later, when the error in even a single step is unbounded by Eq. (7), this can in some cases dominate the global error, rendering the use of a higher-order scheme pointless.

In practical applications, with interpolated velocity fields, the derivatives are not always continuous. For example, a common  
240 choice in the LCS literature appears to be a variable-timestep integrator of order 4 and 5 (see, e.g., Ali and Shah (2007); Shadden et al. (2010); Beron-Vera et al. (2010); Maslo et al. (2020)). Theoretically, seventh-order spline interpolation, yielding five continuous derivatives, are required for the error estimates in the stepsize control routine to hold. However, higher-order spline interpolation is more computationally demanding, and in practice cubic spline interpolation appears to be a common choice. It is also worth noting that, in general, spurious oscillations become increasingly problematic with increasing spline  
245 order.

For such cases, there exist strategies to deal with the discontinuities in the right-hand side or (more commonly in our case) its derivatives (Hairer et al., 1987, p. 181). Three possible strategies for dealing with ODEs with discontinuities are outlined by Hairer et al. (1993, pp. 197–198):

- I Ignore the discontinuity, and let the variable-stepsize integrator sort out the problem.
- 250 II Use an integrator with an error control routine specifically designed to detect and handle discontinuities (see, e.g., Enright et al. (1988); Dieci and Lopez (2012)).
- III Use information about the position of the discontinuity to stop and restart integration at that point.

Given that the issue of interpolation and integration is not typically discussed in great detail in applied papers on Lagrangian oceanography, one assumes that most authors implicitly select the first strategy. However, as pointed out by Hairer et al. (1987,  
255 p. 181), this is neither the most accurate, nor the most numerically efficient, approach.

### 3.2 Analytical example

To illustrate the effect of discontinuities in the derivative of the right-hand side, we consider the following ODE:

$$\dot{x} = |\sin(\pi t)|, \quad x(t=0) = 0. \tag{16}$$

In this case, the right-hand side itself is continuous, but its derivative is discontinuous at  $t = 1$ . This equation has the analytical  
260 solution

$$x(t) = \int_0^t |\sin(\pi s)| \, ds, \tag{17}$$

and if we consider as an example the solution at time  $t_N = 2$ , we find  $x(t_N) = 4/\pi$ . Since the exact solution is known, we can find the error in our numerical solutions by using the exact result as a reference. Hence, we can investigate the convergence of our numerical integration scheme, by considering the error as a function of the timestep,  $h$ .

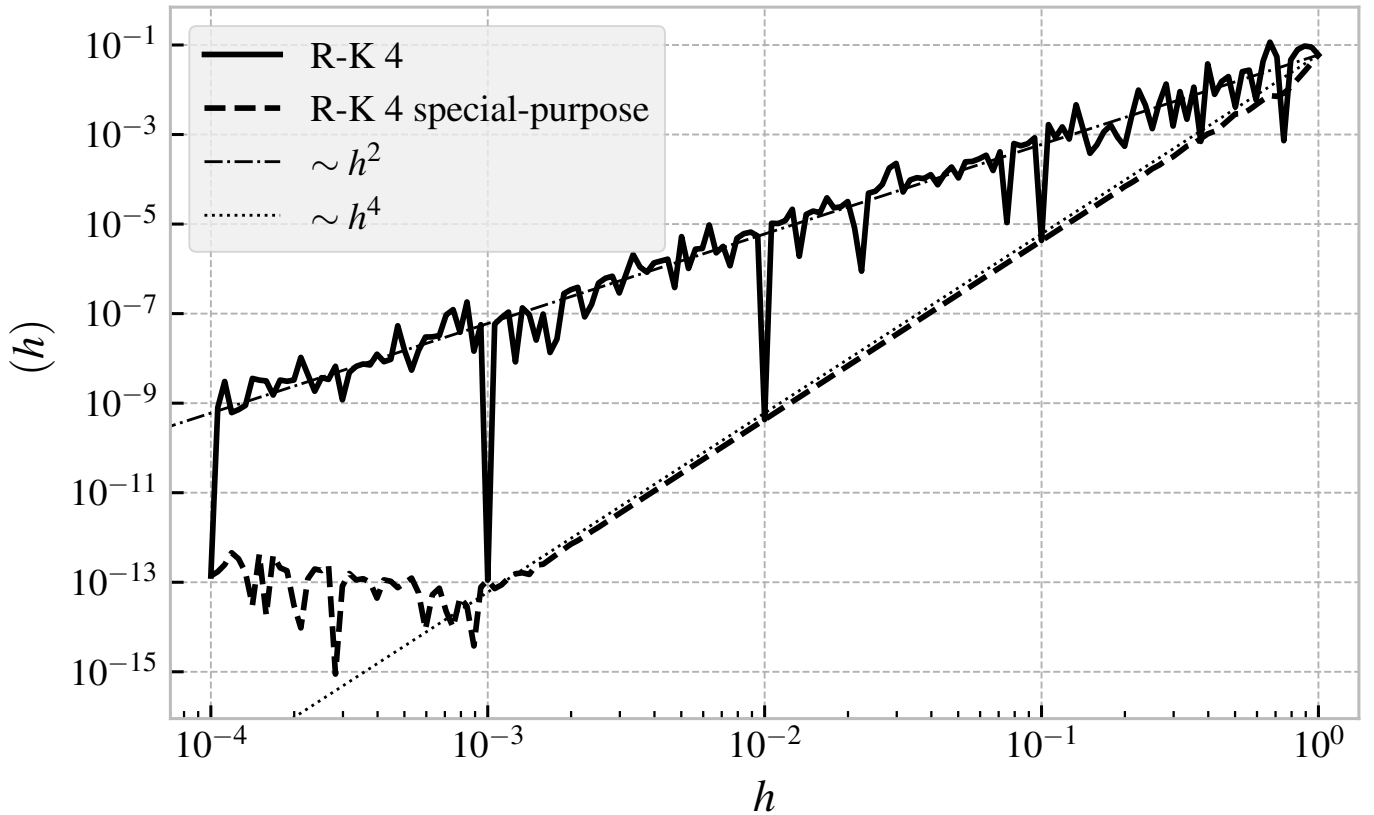


**Figure 2.** Global error in the numerical solution of the initial value problem given by Eq. (16), at  $t_N = 2$ . The solutions have been calculated with 161 different timesteps,  $h$ , logarithmically spaced from  $10^{-4}$  to 1, using the 4th-order Runge-Kutta integrator, and a special-purpose modification of the same, that stops and restarts the integration exactly at the discontinuity at  $t = 1$ . The two thin lines are included to indicate the order of convergence, and are proportional to  $h^2$  (dash-dotted line) and  $h^4$  (dotted line).

265 In Fig. 2, we show the global error in the solution as a function of timestep,  $h$ , for the 4th-order Runge-Kutta integrator (continuous black line). The error has been calculated for 161 logarithmically spaced timesteps from 1 to  $10^{-4}$ . Of these 161 timesteps, only 1,  $10^{-1}$ ,  $10^{-2}$ ,  $10^{-3}$ , and  $10^{-4}$  will evenly divide an interval of length 1. This is significant, as we observe that the error scales approximately as  $h^4$  for the timesteps 1,  $10^{-1}$ ,  $10^{-2}$ , and  $10^{-3}$ , while for the other timesteps it follows a slower  $h^2$  scaling. (Note that at  $h = 10^{-4}$ , the error is dominated by roundoff error (see Appendix A1), which adds up to about  
 270  $10^{-13}$  after 20 000 steps (Press et al., 2007, p. 10).)

The reason for this behaviour is the discontinuity at  $t = 1$ . For those timesteps that divide an interval of length 1 into an integer number of steps, the integration will be stopped and restarted *exactly* at the discontinuity in the derivative of the right-hand side at  $t = 1$ . Therefore, the error bound (Eq. (7)) holds, since the method does not step across the discontinuity. Stopping and restarting at discontinuities is precisely what Hairer et al. (1993, pp. 197–198) recommends in strategy III discussed in

275 Section 3.1 above, and in this sense, isolated discontinuities in the derivatives are easy to handle, if it is known *a priori* where they are.

Inspired by this result, we have designed a special-purpose version of the 4th-order Runge-Kutta integrator, specifically for this problem with a discontinuity at  $t = 1$ . It is identical to the regular one in every way, except that if  $t < 1 < t + h$ , it divides that step into two steps, of length  $1 - t$  and  $h - (1 - t)$ , such that the integration is always stopped and restarted at  $t = 1$ .

280 The global error as a function of timestep for this special-purpose integrator is also shown in Fig. 2 (dashed line), and we observe that it follows very closely the expected  $h^4$  scaling, until the point where roundoff error starts to dominate. The additional computational expense of the special-purpose integrator is completely negligible in this case, as it takes at most one additional step compared to the regular 4th-order Runge-Kutta method, but as we see, it can increase the accuracy by several orders of magnitude. In the next section, we apply this idea to variable-timestep integrators for trajectory calculation in  
285 interpolated vector fields.

### 3.3 Special-purpose integrators for interpolated velocity fields

In terms of the three strategies for dealing with discontinuities (see Section. 3.1) we will investigate a hybrid approach in this paper. We will use information about the location of the discontinuities in the time dimension (strategy III), and leave the error control routine to deal with the problem in the spatial dimensions (strategy I). The reason for this choice is mainly  
290 pragmatic: For a particle trajectory,  $\mathbf{x}(t)$ , time is the independent variable, and it is very easy to stop and restart integration at “cell boundaries” in the time direction. Doing the same in the spatial dimensions requires detection of boundary crossings, dense output from the integrator, and a bisection-scheme to identify the time at which the boundary is crossed (Hairer et al., 1993, pp. 188–196).

We will take as our starting point variable-timestep Runge-Kutta methods, as these are commonly used and generally quite  
295 efficient, and the timestep adjustment routine outlined in Section 2.3. We then modify the timestep adjustment routine to make sure the integration is always stopped and restarted at a cell boundary in time. We assume that the input data is given as snapshots of a vector field at a list of known times,  $T_i$ . Depending on the degree of interpolation, the (higher) partial derivatives of the interpolated vector field along the time dimension will thus have discontinuities at times  $T_i$ .

The variable timestep integrator calculating the trajectory will make steps, from position  $\mathbf{x}_n$ , at time  $t_n$ , to position  $\mathbf{x}_{n+1}$ , at  
300 time  $t_{n+1} = t_n + h_n$ . Then, if we have  $t_n < T_i < t_n + h_n$ , for any  $T_i$ , i.e., if the integration is about to step across a discontinuity in time, the timestep,  $h_n$ , is adjusted such that

$$h_n = T_i - t_n. \tag{18}$$

After that, integration and error control proceeds as normal. If  $h_n$  is set to  $T_i - t_n$ , then a step to that time is calculated. The error is then checked, as described in Section 2.3. If the error is found to be too large according to the selected tolerance, the  
305 step is rejected,  $h_n$  is further reduced, and the step is attempted again. In the opposite case, the step is accepted, and time and position is updated to  $t_{n+1}$  and  $\mathbf{x}_{n+1}$ . At this point, the timestep is reset to the original value of  $h_n$ , to avoid the integration

proceeding with an unnecessarily short timestep after the discontinuity has been crossed. For any step that does not cross a discontinuity in time, the integrator behaves exactly like the regular version.

## 4 Numerical Experiments

310 The aim of the numerical experiments is to investigate the practical implication of different combinations of interpolation and integration schemes, and to compare the special-purpose integrators described in Section 3.3 with their standard counterparts, as well as with fixed-step Runge-Kutta methods. In the following subsections, we describe the input data, and the setup used to carry out the numerical experiments. We have chosen to consider two-dimensional (horizontal) transport only, using the surface layer of the modelled current data. The current velocity field is interpolated in three dimensions (two spatial dimensions plus  
315 time), using the same degree of interpolation in all three dimensions.

In order to allow the interested reader to reproduce our results, we provide the Fortran code used to run the simulations, the ocean current data used, and the jupyter notebooks that were used to analyse the data (Nordam, 2020). These can all be found on github<sup>1</sup>, under an open-source license. In order to reduce the file size of the current data, the extents of the original datasets were reduced, and unused variables were deleted from the files. The domains of the reduced datasets are shown in Fig. 3. All  
320 the datasets were originally downloaded on the netCDF format from the ocean and ice section of the THREDDS server of the Norwegian Meteorological Institute<sup>2</sup>.

### 4.1 Ocean Currents

The datasets used were obtained from the Norwegian Meteorological Institute, and were taken from the following model setups:

- 325
- Arctic20km (20 km horizontal resolution, 1 h timestep),
  - Nordic4km (4 km horizontal resolution, 1 h timestep),
  - NorKyst800m (800 m horizontal resolution, 1 h timestep).

The dimensions of the datasets are  $x$ ,  $y$ ,  $z$  and  $t$ , with the  $xy$  plane defined in a polar stereographic projection, giving a regular (constant spacing) quadratic grid in the horizontal plane. The current velocity field is provided as vector components on the  $xy$  basis (as opposed to, e.g., an East-North basis). In our simulations, we track particle positions in meters, using the  $xy$   
330 coordinate system of the polar stereographic projection of the datasets. This allowed us to use the vector components directly from the datasets, with no rotation or other conversion. All error measurements are calculated from Euclidean distances in the  $xy$  plane.

---

<sup>1</sup>[github.com/nordam/ODE-integrators-for-Lagrangian-particles](https://github.com/nordam/ODE-integrators-for-Lagrangian-particles)

<sup>2</sup><https://thredds.met.no/thredds/fou-hi/fou-hi.html>

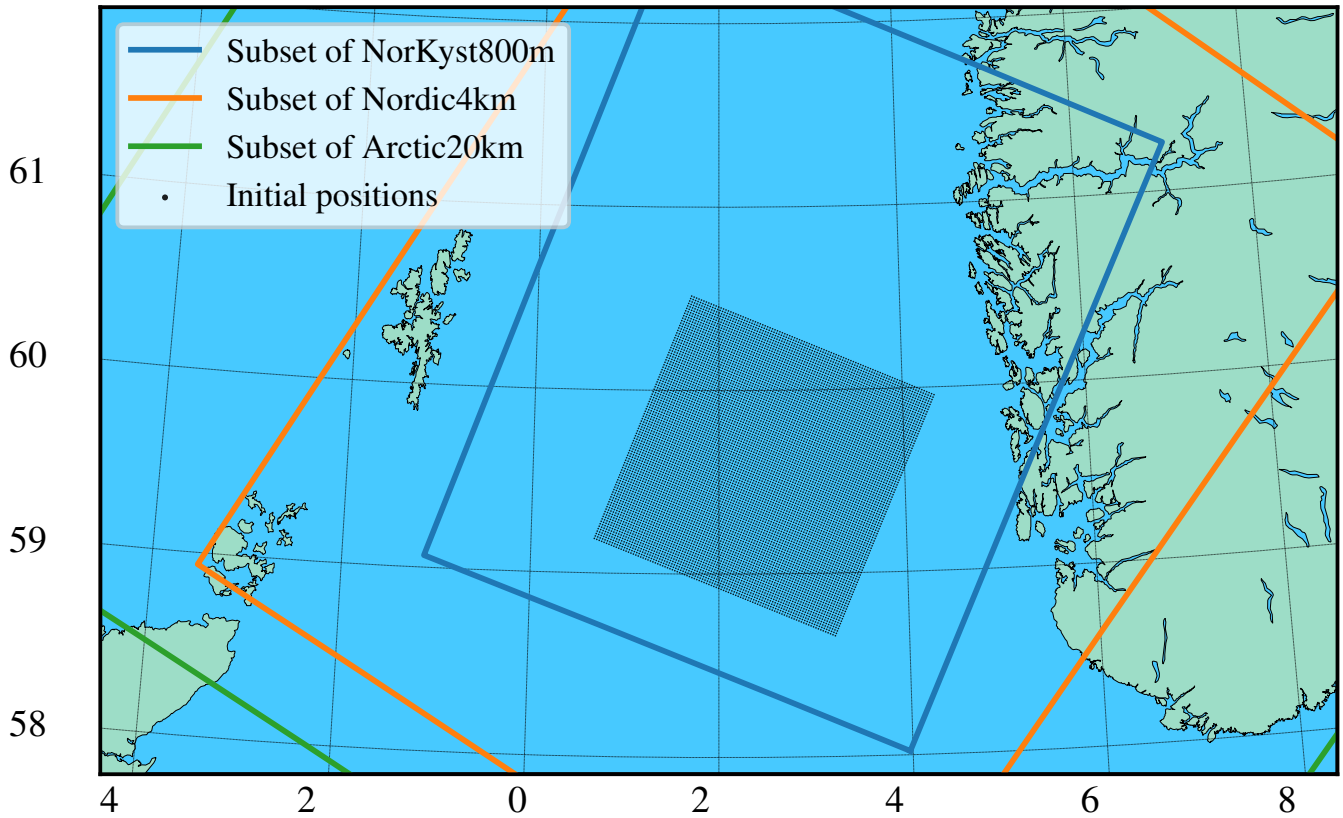


**Figure 3.** Map showing the outline of the three datasets considered, as well as the initial positions of the tracers used in the numerical experiments.

## 4.2 Initial conditions

335 The initial conditions for the trajectory calculations were chosen to be  $100 \times 100$  points off the coast of Norway, placed on a regular quadratic grid with grid spacing of 1600 m, as shown in Fig. 3. The same initial conditions were used for all three datasets. Roughly the easternmost half of the initial positions are within the Norwegian coastal current (see, e.g., Sætre (2005)), and are predominantly transported northward along the coast. The trajectories were started at midnight on February 8, 2017, and integrated for 72 hours. All the particles remain inside the smallest domain (the 800 m resolution setup, see Fig. 3) throughout  
 340 this period. [The final positions are shown in Fig. 4, for each of the three different datasets.](#)

## 4.3 Reference solutions

As we wish to estimate the global error of our numerical solutions, when the true solutions are unknown, we need to establish highly accurate numerical solutions for all 10000 initial conditions, to use as a reference. Reference solutions must be established for each dataset, as they will in general give different [transport trajectories](#). Additionally, reference solutions must also

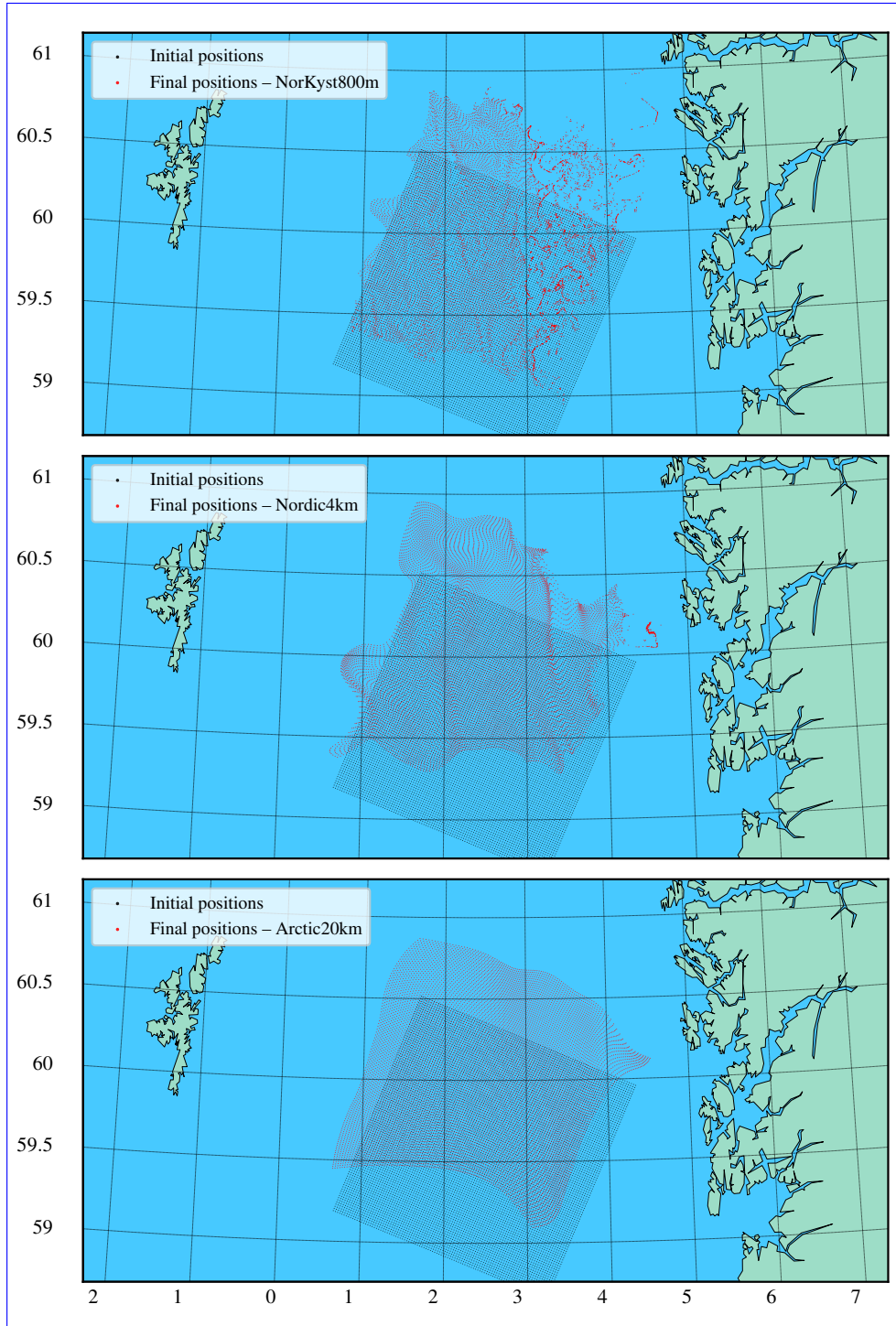


**Figure 4.** The figure shows the initial and final positions of the 10000 particles, for the three different datasets. The initial positions are the same, but the final positions differ. The average transport is towards the north in all cases, but the higher-resolution currents show more eddy activity, particularly in the eastern region which falls within the Norwegian Coastal Current (see, e.g., Sætre (2005)). These plots show the positions calculated with cubic interpolation, 4th-order Runge-Kutta, and a timestep of 1 s. Results obtained with the other methods appear visually identical at this scale.



345 be established for each interpolation scheme, as they will also in general give different trajectories. Hence, for three datasets and three interpolation schemes, we need nine different sets of reference solutions.

We point out that we here talk about reference solutions in a purely numerical sense, as the most mathematically accurate solution of the initial-value problem given by an initial position and a discrete velocity field with a specified interpolation scheme. Which of the datasets and interpolation schemes that most accurately reproduce the trajectories of true Lagrangian drifters in the ocean is a different question, outside the scope of this investigation.

For numerically obtained reference solutions to be useable in calculating error estimates, they need to be significantly more accurate than any of the numerical solutions that are to be evaluated. As an example, consider a fixed-step integrator, and let the numerical solution at time  $t_N$ , calculated with a timestep  $h$ , be  $\mathbf{x}_N(h)$ , and let the true (but usually unknown) solution at time  $t_N$  be  $\mathbf{x}(t_N)$ . Furthermore, assume that a reference solution  $\mathbf{x}_N(h_{\text{ref}})$  has been calculated with a very short timestep  $h_{\text{ref}}$ .

355 Then, the error in the reference solution, relative to the true (but unknown) solution, is given by

$$E_{\text{ref}} = \mathbf{x}_N(h_{\text{ref}}) - \mathbf{x}(t_N). \quad (19)$$

Similarly, the error in a solution calculated with a longer timestep,  $h$ , is

$$E(h) = \mathbf{x}_N(h) - \mathbf{x}(t_N). \quad (20)$$

When we estimate the error by purely numerical means, we do not know the true solution,  $\mathbf{x}(t_N)$ . Instead, we use the reference solution in place of the true solution, and calculate an estimate of the error, given by

$$\begin{aligned} \bar{E}(h) &= \mathbf{x}_N(h) - \mathbf{x}_N(h_{\text{ref}}), \\ &= E(h) - E_{\text{ref}}. \end{aligned} \quad (21)$$

Hence, we see that the numerical estimate,  $\bar{E}(h)$ , of the global error, is only a good estimate if  $E_{\text{ref}} \ll E(h)$ .

To verify that the errors in the reference solutions are indeed much smaller than any of the other errors we wish to estimate, we consider the convergence of the numerically estimated error. The details of the analysis to identify reference solutions are shown in Appendix A. We found that the most accurate solutions were obtained with the 4th-order Runge-Kutta integrator, using a fixed, short timestep. The timestep that yielded the most accurate solutions varied, depending on the dataset and the order of interpolation. The results are given in Table A2.

#### 4.4 Implementation

To allow easy testing of different combinations of datasets, interpolators and integrators, in a setting relevant for marine transport applications, a simple Lagrangian particle transport code was written in Fortran. All the integrators were implemented as described in Sections 2.2, 2.3, and 3.3, and in the references given. The netCDF library for Fortran<sup>3</sup> was used to read ocean current data, and interpolation was done using the library bspline-fortran<sup>4</sup> (Williams, 2018). Our implementations of the different integrators, and all the code used to run the simulations, are freely available on github<sup>5</sup>.

<sup>3</sup>[www.unidata.ucar.edu/software/netcdf/docs-fortran/](http://www.unidata.ucar.edu/software/netcdf/docs-fortran/)

<sup>4</sup>[github.com/jacobwilliams/bspline-fortran](https://github.com/jacobwilliams/bspline-fortran)

<sup>5</sup>[github.com/nordam/ODE-integrators-for-Lagrangian-particles](https://github.com/nordam/ODE-integrators-for-Lagrangian-particles)

At the start of the simulations, subsets of the ocean current datasets were loaded from file. The horizontal extent of the  
375 subsets are shown in Fig. 3, along with the initial positions of the particles. We used only the surface layer of the datasets, and  
data spanning 5 days. The subsets were selected to cover the entire simulation period in time, and the entire horizontal extent  
of the particle trajectories, ~~with some padding on all sides~~ extending some cells in all directions to avoid edge-effects in the  
spline interpolation. Data points that were on land were set to 0 current velocity. No special steps were taken to handle the  
coastline, although the initial conditions were chosen to avoid particles getting stuck in land cells. Note that with higher-degree  
380 interpolation schemes, the fact that we set the currents to zero in land cells will have an effect on one or more of the closest cells  
to the coastline. For applications such as oil spill modelling, where shoreline interactions are important, a different strategy  
might be needed.

The data were passed to the `initialize` method of the derived type `bspline_3d` from the `bspline-fortran` library, along  
with the parameter to select the order of interpolation (note that the order of a spline is 1 plus the polynomial degree, meaning  
385 the order is 2 for linear interpolation, 4 for cubic splines, and 6 for quintic splines). The  $x$  and  $y$  components of the current  
velocity vectors were interpolated separately, and the order of interpolation was always the same along all three dimensions  
( $x, y, t$ ).

We note that this approach constructs a single, global interpolation object, that is used throughout the simulation. It is also  
possible to construct local spline interpolations using only the smallest required number of points, surrounding the location  
390 where the function is to be evaluated ( $2 \times 2 \times 2$  points for linear interpolation,  $4 \times 4 \times 4$  for cubic splines, and  $6 \times 6 \times 6$  for  
quintic). However, this creates additional discontinuities in the derivatives of the right-hand side when switching from one local  
interpolator to the next, as discussed by, e.g., Lekien and Marsden (2005).

During the simulations, the trajectory of each particle was calculated independently of all others. For the variable-step  
integrators, this means that each particle had its own timestep. It is also possible to apply the variable-step integrators to all  
395 particles simultaneously, with the same timestep. However, due the local variability of the ocean currents, it seemed more  
reasonable to treat the particles individually, allowing the variable-step integrators to adapt to local conditions for each particle.

## 5 Results and Discussion

The main results are presented as a work-precision diagram, in Fig. 5. The figure shows the median relative global error  
over all 10000 particles, as a function of number of evaluations of the right-hand side of the ODE (including rejected steps).  
400 The relative global error is calculated as the normalised distance between the endpoint of each trajectory, and that of the  
corresponding reference solution (see Section. 4.3 and Appendix A). See also Fig. B1, where the range of errors is shown.

Number of evaluations of the right-hand side was chosen as a measure of work, as it is more objective than the runtime of  
the simulation, which would depend on the particular machine used to run the simulations, and also be more susceptible to  
somewhat random variations. However, for the interested reader we show the error as a function of runtime in Fig. B2.

405 ~~We note that higher-order~~ While we analyse the results in terms of number of function calls, we note that higher-degree  
interpolation is more computationally costly than ~~lower-order interpolation.~~ For the lower-degree interpolation. This means

that the same number of evaluations will take more time if a higher degree of interpolation is used. We found that for the simulations done with the fixed-step 4th-order Runge-Kutta integrator, the simulations with cubic spline interpolation took on average four to five times longer than those with linear interpolation, and the simulations with quintic spline interpolation took on average three to four times longer than those with cubic spline interpolation. As an a concrete example, calculating the trajectories of 10000 particles, for 72 hours, with a 10 minute timestep with the 4th-order Runge-Kutta integrator, took 11 seconds with linear interpolation, 51 seconds with cubic interpolation, and 177 seconds with quintic interpolation. The numbers were essentially the same for all three datasets (800 m, 4 km and 20 km). These times cover only the trajectory calculation itself, not file I/O or the construction of the global interpolator object.

The fixed-step integrators were run with the range of timesteps shown in Table 1. Note that all of these steps evenly divide the 3600 s interval of the data, making sure that the integration is always stopped and restarted at a cell boundary in the time dimension (see discussion in Section 3).

**Table 1.** Timesteps and tolerances used in the numerical experiments.

Timesteps [s]	120, 180, 300, 450, 600, 900, 1200, 1800, 3600.
Tolerances	$10^{-4}$ , $10^{-5}$ , $10^{-6}$ , $10^{-7}$ , $10^{-8}$ , $10^{-9}$ , $10^{-10}$ , $10^{-11}$ , $10^{-12}$ , $10^{-13}$ , $10^{-14}$ .

The tolerances used with the variable-step integrators are also shown in Table 1, with  $T_A = T_R$  (see Section 2.3). Note that in the coordinate system used, the particle positions are all of the order  $10^6$  m, meaning that the relative tolerance dominates in practice (see Eq. (10)). Both the regular and the special-purpose variable-step integrators were used with the same tolerances, but we note that the special-purpose integrators are by design unable to take steps longer than the interval on which the data is given. Hence, for the higher tolerances (allowing larger errors), the special-purpose integrators would default to fixed-step integration with a timestep of 3600 s (for the datasets used here).

We observe from Fig. 5 that the most efficient choice of integrator, in the sense of fewest evaluations of the right-hand side for a given accuracy, depends on the desired accuracy, the order of the interpolation, and the spatial resolution of the dataset. We will discuss these points in turn.

## 5.1 Fixed step integrators

Variable-step integrators are normally the most efficient choice for general ODE problems. However, we see that for finding tracer trajectories from interpolated velocity fields, fixed-step integrators are in some cases a better choice than regular variable-step methods. Considering for example cubic spline interpolation (Fig. 5, middle row), we see that 4th-order Runge-Kutta almost always gives better accuracy for the same amount of work, relative to all three regular variable-step integrators. The only exception is for very small errors, for the 800 m dataset, where Dormand-Prince 5(4) has a small advantage. Similarly for

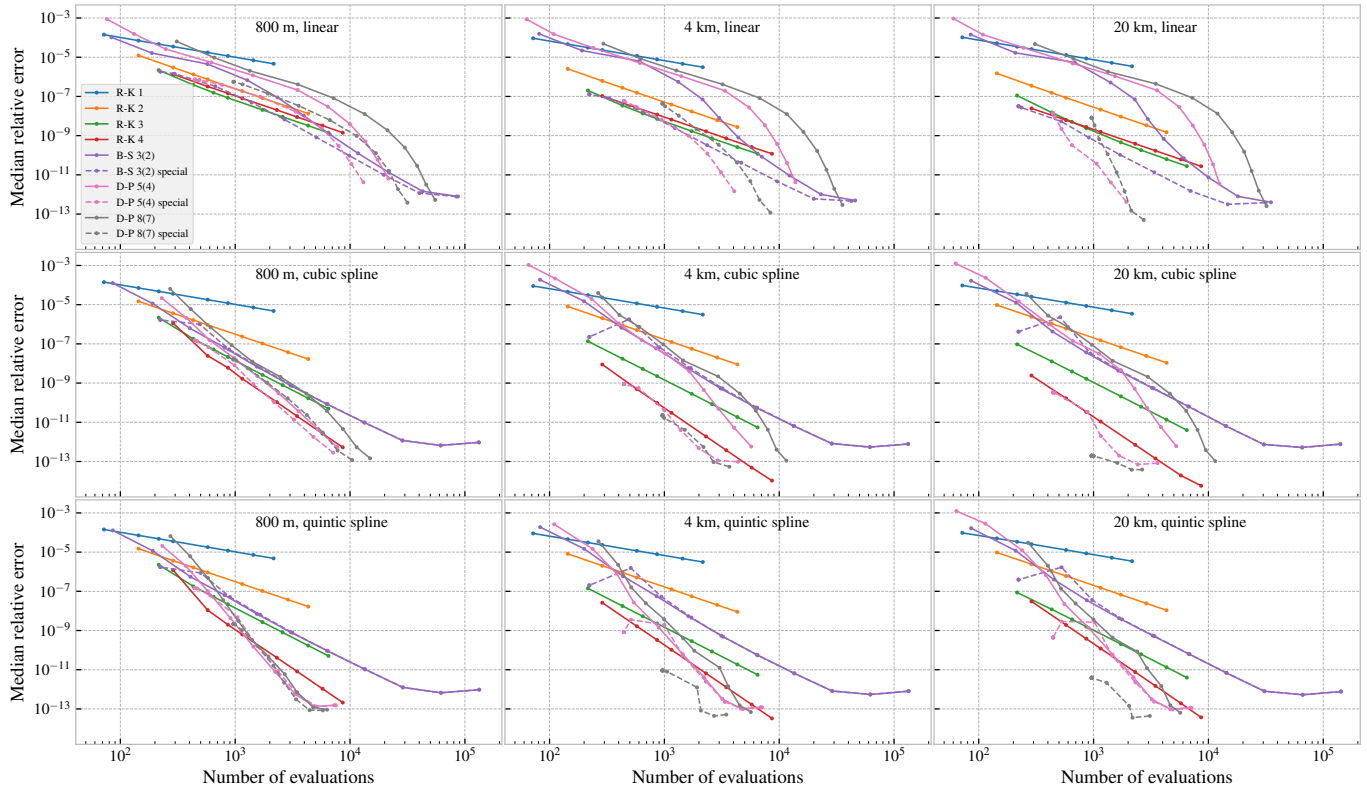


**Figure 5.** Relative global error (relative to the reference solution) as a function of number of evaluations of the right-hand side. Note that the special-purpose integrators are (by design) unable to make longer steps than the interval on which the data are provided. This means some of the simulations with higher tolerance (allowing larger errors) have in practice defaulted to fixed-step simulation with a timestep of 3600 s, making several of the data points identical. This is most readily observed for the special-purpose Dormand-Prince 8(7) integrator, in the lower right panel.

linear interpolation (Fig. 5, top row), the 3rd- and 4th-order fixed-step methods outperform the regular variable-step methods, except if very small errors are required.

435 The special-purpose variants of the variable-step integrators, particularly Dormand-Prince 5(4) and 8(7), perform better than the fixed-step methods in most cases, though not always by a large margin. The reason for the relatively strong performance of the fixed-step integrators is that the chosen timesteps evenly divide the 3600 s intervals of the datasets. Hence, the fixed-step integrators will stop and restart integration at the discontinuities in time, just like the special-purpose integrators (see Section 3.3). For an illustration of the effect of choosing timesteps that do *not* evenly divide the temporal grid spacing of the dataset, see Nordam et al. (2017, Fig. 18).

440

We also note that for the case of linear interpolation, the 3rd-order Runge-Kutta integrator actually performs slightly better than the 4th-order, particularly for the smaller errors. The reason for this is that the lack of continuous derivatives means the 4th-order method does not achieve 4th-order convergence. As the 3rd-order method uses one fewer evaluation of the right-hand

side per step, it therefore has an advantage in terms of computational effort. It is also worth pointing out that the 2nd-order  
445 Runge-Kutta method considered here, known as the explicit trapezoid method, has the advantage that it uses no intermediate  
points in time. Since it only evaluates the right-hand side at times  $t_n$  and  $t_{n+1}$ , it is possible to dispense with interpolation  
in time entirely if one selects the integration timestep,  $h$ , to be equal to the temporal grid spacing of the data. Note that this  
requires reasonably high temporal resolution of the dataset, which may not always be practical.

## 5.2 Variable-step integrators

450 As a background for discussing the effect of horizontal resolution on our results, we recall that all the three datasets used  
have a temporal resolution of 1 hour. This means that the particle trajectories will cross a cell boundary in the time-dimension  
(and thus a discontinuity in the (higher) derivatives of the right-hand side) every hour. The average current speed for the time  
and area studied is approximately 0.2 m/s in all three datasets. Hence, we find that a particle that moves in the velocity field  
defined by the dataset at 800 m spatial resolution will cross a spatial cell boundary approximately once every hour on average.  
455 For the dataset with 4 km resolution, this will only happen 1/5th as often, and for the 20 km dataset, only 1/25th as often.  
These are only crude estimates, but we can nevertheless conclude that for the low-resolution datasets, the errors picked up at  
the discontinuities in time will be more important than those in space, while for the high-resolution (800 m) dataset, the two  
will be of similar importance.

Looking at the results presented in Fig. 5, we find that they support these observations. Considering first the case of linear  
460 interpolation, we see that for the 20 km dataset (Fig. 5, upper right panel), there is a considerable (several orders of magnitude)  
reduction in error in the special-purpose integrators, compared to the regular variable-step integrators for a given number of  
evaluations. Recall that the only difference between these is that the special-purpose integrators stop and restart the integration  
at every cell boundary along the time dimension (see Section 3.3). For the 800 m dataset (Fig. 5, upper left panel) on the other  
hand, there is less (up to about an order of magnitude) difference between the regular and special variable-step integrators. This  
465 is presumably because the discontinuities in time do not dominate the error as much in this case.

Looking next at the results for cubic spline interpolation (Fig. 5, middle row), we notice that the results for the regular and  
special-purpose versions of the Bogacki-Shampine 3(2) integrator are now practically identical. For the Dormand-Prince 5(4)  
and 8(7) integrators, the special-purpose variants are far more accurate than the standard counterparts. This is particularly true  
for the 4 km and 20 km datasets, where the difference is several orders of magnitude.

470 Presumably, the reason why the standard and special-purpose variants of the Bogacki-Shampine 3(2) integrator give more  
or less identical results for cubic interpolation is the smoothness of the velocity field. It seems the interpolated field is now  
sufficiently smooth that the method is now third-order consistent. Strictly speaking, this is unexpected. A cubic spline inter-  
polation will have continuous second derivatives, and discontinuous third derivatives. This means that the Bogacki-Shampine  
3(2) integrator can indeed be expected to be second-order consistent, but the conditions for the third-order consistency are not  
475 satisfied.

Using quintic spline interpolation (Fig. 5, bottom row), the special-purpose variant of the Dormand-Prince 8(7) integrator  
performs better than all the other methods by at least an order of magnitude. We also find that the results for the regular and

special-purpose versions of the Dormand-Prince 5(4) integrators are more or less identical. As above, this was not entirely expected, since a quintic spline has only four continuous derivatives, not the five that are theoretically required for the local error of a 5th-order method to be bounded by Eq. (7).  
480

To understand the large differences in number of function evaluations between the standard and the special-purpose integrators, we look at the fraction of rejected steps. For the different integrators and interpolators, and a fixed tolerance of  $T_A = T_R = 10^{-10}$ , these fractions are given in Table 2. Rejected steps represent wasted computational effort, since a rejected step requires as many evaluations of the right-hand side of the ODE as an accepted step, without advancing the integration.

485 The results shown in Table 2 further support the conclusions we drew from Fig. 5 above. For those cases where the order of interpolation is less than the theoretical requirements of the integrator, the special-purpose integrators significantly reduce the fraction of rejected steps. The difference is also largest for the 20 km dataset, as discussed previously. This can be seen particularly for the Dormand-Prince 8(7) integrator with cubic and quintic interpolation, where the rejected fraction falls to almost nothing for the special-purpose variant. The same, but to a lesser degree, is seen for the Dormand-Prince 5(4) integrator,  
490 with linear and cubic interpolation. On the other hand, for the Bogacki-Shampine 3(2) integrator, with cubic and quintic interpolation, we see that there is essentially no difference between the regular and special variants, as the velocity field is sufficiently smooth for the error control routine not to detect any increased local error at the boundary crossings.

The largest improvement in accuracy for the special-purpose integrators is thus seen with linear interpolation, but they can also be advantageous with cubic interpolation. With quintic interpolation, only the special-purpose (8)7 integrator has  
495 an advantage over its regular counterpart. However, the relative error of the special (8)7 method with quintic interpolation is comparable to the (5)4 method with cubic interpolation. While the solutions will be different with different interpolation schemes, it is possible that overshooting due to a high order interpolation method without any additional accuracy implies that the (8)7 method is not a good choice for Lagrangian oceanography. Note also that the quintic interpolation scheme is 3-4 times as computationally expensive as the cubic, for each evaluation of the right-hand side.

### 500 5.3 Diffusion

As mentioned in Section 2, we have considered pure advection, ignoring diffusion. Calculating trajectories with pure advection by a deterministic velocity field is common in several applications, perhaps most notably for identification of LCS (see, e.g., Haller (2015); Allshouse et al. (2017); Duran et al. (2018)). Other examples include the use of backwards trajectories to identify source regions for particles ending up in the sediments (Van Sebille et al., 2015), and analysis of Lagrangian pathways to study the source and history of water parcels reaching a particular upwelling zone (Rivas and Samelson, 2011). In general, simulating diffusion in Lagrangian oceanography (or meteorology) may introduce a complication that encourages some studies to compute trajectories without diffusion: Lagrangian motion becomes ambiguous when diffusive mixing is simulated, because the identity of a fluid parcel is lost. On the other hand, ignoring small-scale mixing may also be problematic. One approach to this problem is to supplement purely advective trajectories with along-path changes in parcel properties, as discussed in Rivas and Samelson (2011).  
505  
510

**Table 2.** Fraction of steps rejected, averaged over all 10000 trajectories, with a duration of 72 hours, for each combination of interpolation scheme and variable-stepsizes integrator, for all three datasets, and a fixed tolerance of  $T_A = T_R = 10^{-10}$  (see Section 2.3).

Resolution	Integrator	Linear	Cubic	Quintic
20 km	B-S 3(2)	0.334	0.017	0.018
20 km	B-S 3(2) special	0.067	0.016	0.018
20 km	D-P 5(4)	0.588	0.486	0.251
20 km	D-P 5(4) special	0.084	0.113	0.156
20 km	D-P 8(7)	0.608	0.558	0.482
20 km	D-P 8(7) special	0.152	0.000	0.000
4 km	B-S 3(2)	0.309	0.023	0.024
4 km	B-S 3(2) special	0.095	0.022	0.024
4 km	D-P 5(4)	0.587	0.436	0.247
4 km	D-P 5(4) special	0.289	0.115	0.158
4 km	D-P 8(7)	0.609	0.554	0.394
4 km	D-P 8(7) special	0.379	0.012	0.019
800 m	B-S 3(2)	0.266	0.016	0.016
800 m	B-S 3(2) special	0.161	0.016	0.016
800 m	D-P 5(4)	0.580	0.294	0.217
800 m	D-P 5(4) special	0.490	0.159	0.152
800 m	D-P 8(7)	0.615	0.468	0.237
800 m	D-P 8(7) special	0.545	0.269	0.124

However, for many other applications diffusion must be included. Solving the advection-diffusion equation with a particle method amounts to numerical solution of a stochastic differential equation (SDE), instead of an ODE. A range of different SDE schemes exist, and the details differ, but all such schemes involve adding a random increment at each timestep. If the random increment is far larger than the local numerical error in each step, then the numerical error in the advection is probably of limited practical importance. The details will depend on the application, and we encourage experimentation. A detailed description of numerical SDE schemes is outside the scope of this study, but the interested reader may find it useful to refer to, e.g., Kloeden and Platen (1992), Spivakovskaya et al. (2007), and Gräwe (2011).

#### 5.4 Summary

We have seen that the special-purpose integrators are more efficient than their regular counterparts in almost all cases, and sometimes they deliver several orders of magnitude improvement in accuracy at the same computational cost. There are two different effects that give the special-purpose integrators their advantage in accuracy and efficiency. The first is that they stop

and restart integration exactly at the discontinuities in time, which avoids picking up local errors unbounded by Eq. (7) at those points. The second effect is that they avoid many rejected steps by stopping at the discontinuity, instead of trying to step across.

The regular variable-step integrators will frequently try to step across a discontinuity, only to find that the estimated local error is too large, such that the step must be rejected and retried with a shorter timestep. This process will continue until a timestep is found that is short enough to allow the discontinuity to be crossed with an error that stays within the tolerance. As we see from the results in Table 2, this can lead to a large fraction of rejected steps. Also, recall that the regular variable-step integrators have no information about the location of the discontinuities in time, which means that the probability of stopping and restarting the integration exactly at a discontinuity is essentially zero. For further details, see the discussion in Section 3, as well as Hairer et al. (1987, p. 181) and Hairer et al. (1993, pp. 197–198).

## 6 Conclusions

In this paper, we have investigated how different numerical integrators behave, in combination with different degrees of interpolation, and datasets of different spatial resolution. We have calculated trajectories over 72 hours, from 10000 initial positions, and compared the integrator-interpolator pairs in terms of the error in the final position of each trajectory. We have considered linear, cubic and quintic spline interpolation, along with four fixed-step Runge-Kutta integrators of orders 1 to 4, three commonly used variable-step integrators, and three special-purpose variants of the latter.

The most striking conclusion from ~~the results presented above, our results~~ is that the special-purpose integrators we describe in many cases deliver several orders of magnitude more accurate results, at no additional cost. Alternatively, they can deliver the same accuracy as standard methods, with highly reduced computational effort. This is ~~particularly true~~ achieved by stopping and restarting the integration exactly at the grid points of the dataset along the time dimension. By doing this, we avoid stepping across discontinuities in the (higher) derivatives of the velocity field, and thus we avoid picking up local errors that are unbounded by Eq. (7) at those points.

The benefit is particularly visible for linear and cubic interpolation, and the 4 km and 20 km datasets. The increased efficiency of these integrators should be particularly relevant for long-term simulations, such as studies of global transport of plastics or global climate simulations.

Going more into details, we find that the most efficient choice of integrator depends on the resolution of the dataset, the degree of interpolation, and the desired accuracy. Looking at cubic interpolation (Fig. 5, middle row), we find that the fixed-step 4th-order Runge-Kutta method is in most cases a more efficient choice than a standard variable-step integrator (provided the timestep is selected to evenly divide the interval of the dataset). The difference varies with the resolution of the dataset and the required accuracy, but in some cases the error is two orders of magnitude smaller for the 4th-order Runge-Kutta than the regular Dormand-Prince 5(4) method. This is an interesting result, given that the combination of cubic interpolation and a variable-step integrator such as Dormand-Prince 5(4) or Runge-Kutta-Fehlberg (Hairer et al., 1993, p. 177) appears to be a popular choice. In the case of the 20 km dataset, and to a lesser extent for the 4 km dataset, additional accuracy can be gained by switching to a special-purpose variant of the Dormand-Prince integrators.



555 For linear interpolation, we find that if very small errors are required, the regular variable-step integrators perform better than the fixed-step methods, and in particular the Bogacki-Shampine 3(2) integrator. The special-purpose variable-step methods achieve notable improvements, often being several orders of magnitude more precise. For less strict requirements, the 3rd-order Runge-Kutta method appears to be the best choice. However in all cases, there is a considerable improvement in accuracy with the special-purpose integrators relative to the regular variable-step methods.

560 For quintic spline interpolation, the optimal choice of interpolator again depends on the application. If very small errors are required, the Dormand-Prince 5(4) method appears to be the best performer, or alternatively the special-purpose variant of Dormand-Prince 8(7). If larger errors are acceptable, the 4th-order Runge-Kutta method seems to be the better choice.

It is interesting that if an appropriate fixed step is chosen (i.e., a step that divides the interval between discontinuities in time), the 4th-order Runge-Kutta method is more efficient than the regular Dormand-Prince (5)4 method for all ocean model  
565 resolutions. This is true for any interpolation scheme and accuracies, except linear and quintic interpolations when very small errors are desired. The 4th-order method with a good choice of time step also performs well relative to the special-purpose 5(4) method although the latter may significantly outperform the former with linear and cubic interpolations. The strong performance of the 4th-order Runge-Kutta with all resolutions and interpolation schemes makes it a good practical choice.

To conclude, we have investigated the accuracy of trajectory calculation with 10 different ODE integrators, for 9 different  
570 combinations of current data resolution and order of interpolation. We find that the optimal choice of integrator depends on the interpolation, the resolution, and the required accuracy. In some cases, the most efficient integrator is not the most popular choice in the literature.

We have designed and investigated special-purpose variants of the regular variable-step integrators. Only minimal changes to the code is required, to ensure that integration is always stopped and restarted at discontinuities in time. With this change,  
575 these special-purpose integrators can in some cases increase the accuracy by many orders of magnitude, for the same amount of computational effort. For applications requiring large numbers of trajectories, such as LCS calculations, or for long-term transport calculations, the added accuracy of the special-purpose methods should allow significant reductions in computational expense.

*Code and data availability.* The code used to run the simulations and analyse the results, as well as the three different ocean current datasets,  
580 can be found at [github.com/nordam/ODE-integrators-for-Lagrangian-particles](https://github.com/nordam/ODE-integrators-for-Lagrangian-particles).

## Appendix A: Reference solutions

In order to establish highly accurate reference solutions, which are needed to estimate the error when the true solutions are unknown, an expanded set of timesteps and tolerances were investigated. These are given in Table A1. For each timestep in the expanded set, a solution was calculated with the 4th-order Runge-Kutta method, and for each tolerance in the expanded set,

**Table A1.** Timesteps and tolerances used in establishing reference solutions.

Timesteps [s]	3600, 1800, 1200, 900, 450, 300, 180, 120, 60, 30, 10, 5, 2, 1.
Tolerances	$10^{-4}, 10^{-5}, 10^{-6}, 10^{-7}, 10^{-8}, 10^{-9}, 10^{-10}, 10^{-11},$ $10^{-12}, 10^{-13}, 10^{-14}, 10^{-15}, 10^{-16}, 10^{-17}.$

585 a solution was calculated with the Dormand-Prince 8(7) method, using both the regular and the special-purpose variant. This was done for each of the three datasets, and for each of the three orders of interpolation.

### A1 Roundoff error and truncation error

Every step with a numerical ODE integrator contains some error. The *truncation error* stems from approximations that are made in constructing the integrator, and decreases with timestep. The *roundoff error* comes from the finite-precision representation  
590 of numbers on a computer, and is independent of the timestep. Due to numerical roundoff error, one can not simply assume that the shortest timesteps or smallest tolerance will always give the most accurate answer. As the number of steps increase, the roundoff error will eventually become larger than the truncation error, at which point no accuracy is gained by reducing the stepsize further.

Loosely speaking, a double precision floating point number can store approximately 16 significant digits, and any numerical  
595 operation should be thought of as introducing a roundoff error in the least significant digit (Press et al., 2007, p. 10). This means that any step with an ODE integrator unavoidably introduces a relative error of approximately  $10^{-16}$ . As the timestep is reduced, the numbers of steps increase, and eventually the net contribution of the added roundoff errors will dominate. An example of this can be seen in Fig. 2, where the error of the special-purpose method decreases down to about  $10^{-13}$ , whereafter it begins to increase with further reduction of the timestep.

### 600 A2 Finding the most accurate solutions

In order to establish the most accurate solutions, we compare the 4th-order Runge-Kutta solutions obtained with very short timesteps, and Dormand-Prince 8(7) solutions with very small tolerances. We let the 4th-order Runge-Kutta solutions obtained with timestep  $h$  be given by  $\mathbf{x}_N(h)$ , and the Dormand-Prince 8(7) solutions obtained with relative tolerance  $T_R$  (see Section 2.3) be given by  $\mathbf{x}_N(T_R)$ . We also let the (unknown) true solution be given by  $\mathbf{x}(t_N)$ . Then we consider the relative difference  
605 between these numerical solutions,  $\Delta(h, T_R)$ , given by

$$\Delta(h, T_R) = \frac{|\mathbf{x}_N(h) - \mathbf{x}_N(T_R)|}{|\mathbf{x}_N(T_R)|} \tag{A1a}$$

$$= \frac{|(\mathbf{x}_N(h) - \mathbf{x}(t_N)) - (\mathbf{x}_N(T_R) - \mathbf{x}(t_N))|}{|\mathbf{x}_N(T_R)|}. \tag{A1b}$$

In Eq. (A1b), we have added and subtracted the true (but typically unknown) solution,  $\mathbf{x}(t_N)$ , highlighting that  $\Delta(h, T_R)$  is also equivalent to the difference in the global error of the fixed-step and variable step solutions (see Eq. 6).

610 To evaluate the accuracy of the numerical solutions, we first keep the tolerance,  $T_R$ , fixed, and we plot the median relative difference as a function of timestep,  $h$ . The result is shown in Fig. A1. We observe that for longer timesteps, the relative difference,  $\Delta(h, T_R)$ , goes down with the timestep,  $h$ . Starting from the bottom row of Fig. A1, we observe that for quintic interpolation,  $\Delta(h, T_R)$  scales as  $h^4$  (dashed lines). This is as expected, since a quintic spline has continuous partial derivatives up to order four, as required for the 4th-order Runge-Kutta method to be guaranteed to deliver 4th-order accuracy (see  
615 discussion in Sections 2.1 and 2.4, as well as Hairer et al. (1993, p. 157)). We also observe the same trend for cubic interpolation (Fig. A1, middle row), while for linear interpolation (Fig. A1, top row), we find that the estimated error only goes down proportional to  $h^2$ , due to the lack of continuous derivatives.

For shorter timesteps, we observe that the relative difference,  $\Delta(h, T_R)$ , flattens out and becomes constant. The interpretation of this, in light of Eq. (A1b), is that for the shorter timesteps,  $\Delta(h, T_R)$  is dominated by the error in the variable-step reference  
620 solution, thus appearing to be constant with the timestep  $h$ . Based on this reasoning, we conclude that the most accurate variable-step solutions are obtained with the special-purpose integrator, with a tolerance of  $10^{-13}$ ,  $10^{-14}$ , or  $10^{-15}$ , depending on the dataset and the order of interpolation.

Next, we do the opposite comparison, i.e., we use the 4th-order Runge-Kutta solutions as reference, keep the timestep fixed and look at the relative difference,  $\Delta(h, T_R)$ , as a function of tolerance. The results are shown in Fig. A2. Starting from the  
625 high tolerances, we observe that the relative difference first goes down as the tolerance is reduced. Then, in all cases except the linearly interpolated 800 m dataset, the smallest estimated differences thereafter go up as the tolerance is reduced further. The reason is that the error in the variable-step solutions goes down until at some point the accumulated roundoff errors begin to dominate, and the error increases as the reduced tolerance leads to an increasing number of steps.

From Figs. A1 and A2 together, we conclude that the 4th-order Runge-Kutta solutions for short timesteps are the most  
630 accurate solutions. As we can see from Eq. (A1b), we are essentially considering the absolute value of the difference in the error of the fixed-step solution, and the error in the variable-step solution. Since  $\Delta(h, T_R)$  (Fig. A1) appears constant with timestep (for the shortest timesteps), we conclude that  $\Delta(h, T_R)$  is dominated by the (relatively) large, constant error in the variable-step solution, obscuring the small changes with timestep in the error in the fixed-step solution.

In order to further investigate the relative accuracy of the 4th-order Runge-Kutta solutions, we consider the change in the  
635 solution between two different values of the timestep. First, we list all the timesteps in Table A1, such that  $h_0 = 1$  s,  $h_1 = 2$  s,  $h_2 = 5$  s,  $h_3 = 10$  s, etc. Then we consider the quantity

$$\Delta_{\text{RK4}}(h_i, h_{i+1}) = \frac{|\mathbf{x}_N(h_{i+1}) - \mathbf{x}_N(h_i)|}{|\mathbf{x}_N(h_i)|} \tag{A2a}$$

$$= \frac{|(\mathbf{x}_N(h_{i+1}) - \mathbf{x}(t_N)) - (\mathbf{x}_N(h_i) - \mathbf{x}(t_N))|}{|\mathbf{x}_N(h_i)|} \tag{A2b}$$

As  $h_i$  and  $h_{i+1}$  become smaller, we expect  $\Delta_{\text{RK4}}(h_i, h_{i+1})$  to become smaller as well. Since the global error of a 4th-order Runge-Kutta method (for sufficiently smooth right-hand sides) is  $\mathcal{O}(h^4)$ , we see from Eq. (A2b) that

$$\Delta_{\text{RK4}}(h_i, h_{i+1}) \sim (\mathcal{O}(h_{i+1}^4) - \mathcal{O}(h_i^4)). \quad (\text{A3})$$

In Fig. A3, we plot  $\Delta_{\text{RK4}}(h_i, h_{i+1})$ , as a function of  $h_i$ . For the linearly interpolated datasets, we observe that  $\Delta_{\text{RK4}}(h_i, h_{i+1})$  decreases proportionally to  $h^2$ , since the linearly interpolated right-hand sides are not sufficiently smooth to yield 4th-order convergence, and does not flatten out for small timesteps. Hence, we conclude that the solutions obtained with timestep  $h = 1$  s are the most accurate in this case.

With cubic and quintic interpolation, we see that  $\Delta_{\text{RK4}}(h_i, h_{i+1})$  goes down approximately as  $h^4$ , and eventually flattens out and increases a little for the shortest timesteps. As discussed previously, we interpret this to mean that the accumulated roundoff errors begin to dominate. We find that the smallest difference is obtained with different timesteps for the different datasets. For example, for the 800 m resolution dataset, a timestep  $h = 5$  s appears to be the most accurate, while for the 20 km dataset, a timestep of 30 s appear to give better accuracy.

Based on the analysis described above, we have decided to use the 4th-order Runge-Kutta method to obtain the reference solutions used for the analysis in Section 5. For each dataset and order of interpolation, the reference timestep is chosen based on Fig. A3, and the results are shown in Table A2.

**Table A2.** Timestep used with the 4th-order Runge-Kutta method, to obtain the reference solutions used in Section 5, for each order of interpolation and each dataset.

	800 m	4 km	20 km
Linear	1 s	1 s	1 s
Cubic	5 s	30 s	30 s
Quintic	5 s	30 s	30 s

As a final remark, we mention that it may seem surprising that we are able to obtain higher accuracy with the 4th-order Runge-Kutta method than with the Dormand-Prince 8(7) method. Three things are worth pointing out in this context. First, the timesteps considered here (see Table A1) all evenly divide the 1 hour step of the data, which means that a fixed-step method will always stop and restart the integration at the discontinuities in the time-direction (see discussion in Section 3.1). Second, for the Dormand-Prince 8(7) method to work optimally, the right-hand side of the ODE should strictly have continuous partial derivatives up to order 8, which would require spline interpolation of degree 9. Finally, variable-step methods are generally preferred for their *efficiency*, not purely for their accuracy. As an example, consider the fifth-degree interpolated 800 m dataset. In this case, the presumed most accurate fixed-step solution, with  $h = 5$  s used 207 360 evaluations of the right-hand side, while the most accurate Dormand-Prince 8(7) solution, with a tolerance of  $10^{-14}$ , used 5805 evaluations (including 17% rejected steps).

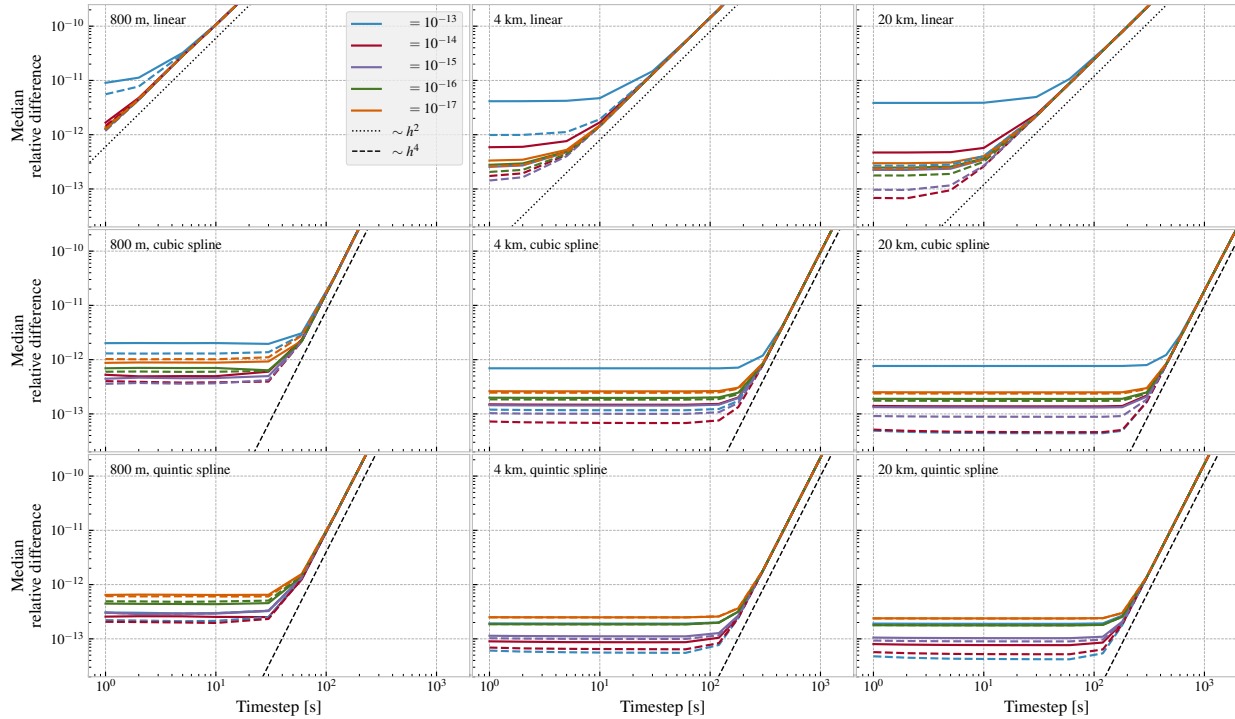


**Figure A1.** Median relative difference (Eq. (A1)) between the 4th-order Runge-Kutta solutions and the Dormand-Prince 8(7) solutions, as a function of the timestep for the Runge-Kutta method, and shown for different tolerances for the Dormand-Prince method. The regular Dormand-Prince 8(7) is shown as continuous lines, and the special-purpose variant as dashed lines.

## Appendix B: [Additional work-precision diagrams](#)

665 [This appendix contains two additional figures, to supplement the work-precision diagram shown in Fig. 5. See Section 5 for further details. First, in Fig. B1, we show the same data as in Fig. 5, that is, the median global error over 10000 trajectories, but with the addition of shaded areas that indicate the range covering 90% of the errors.](#)

670 [Second, Fig. B2 shows the median global error as a function of simulation runtime. The timings were obtained on a desktop workstation with an Intel Xeon 3.3 GHz CPU, running xubuntu 18.04. The code runs on a single core only. As discussed in Section 5, the number of evaluations of the right-hand side of the ODE is a more objective measure of work, as the runtime is susceptible to some random variation \(in particular for the shortest simulations\) due to other processes running on the machine, etc. However, we include the runtimes here as an illustration, as it is practically relevant information.](#)

*Author contributions.* TN wrote the simulation code, and the first draft of the manuscript. Both authors participated in development of ideas, analysis of results, and writing of the final manuscript.

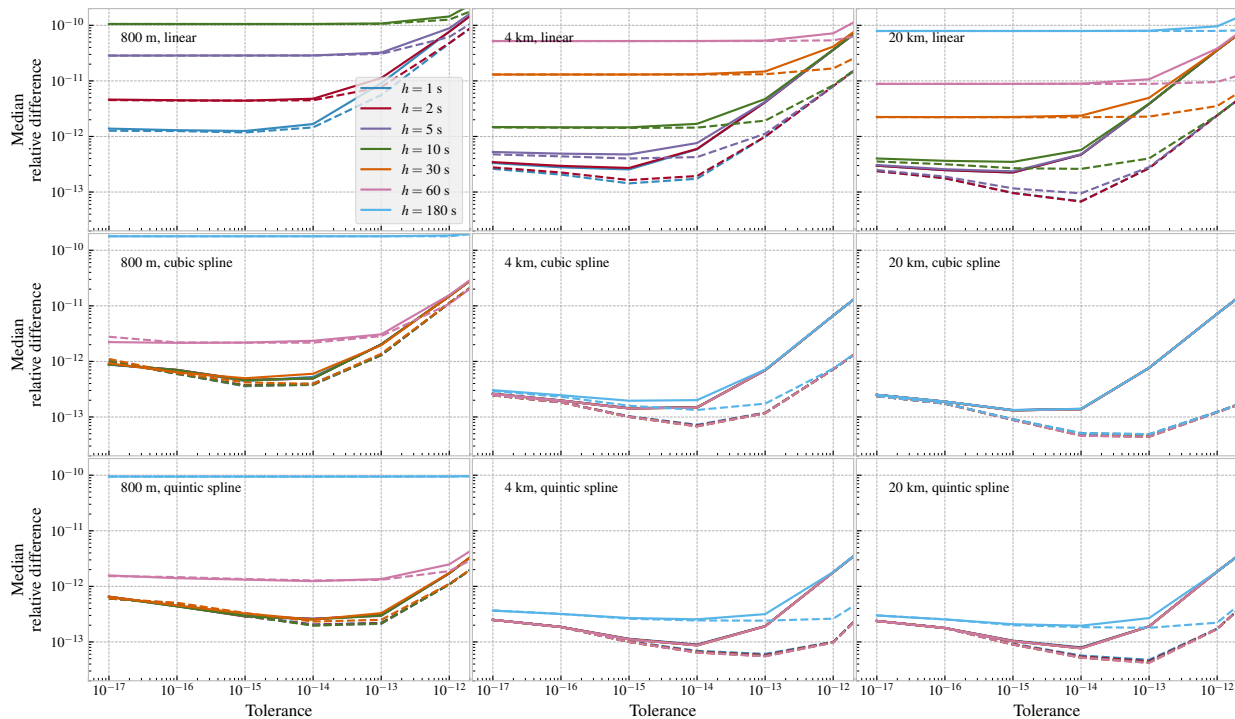


**Figure A2.** Median relative difference (Eq. (A1)) between the Dormand-Prince 8(7) solutions and the 4th-order Runge-Kutta solutions, as a function of the tolerance for the Dormand-Prince method, and shown for different timesteps for the Runge-Kutta method. The regular Dormand-Prince 8(7) is shown as continuous lines, and the special-purpose variant as dashed lines.

675 *Competing interests.* The authors declare that they have no competing interests.

*Acknowledgements.* The work of TN was supported in part by the Norwegian Research Council, through the project INDORSE (267793). TN would also like to thank his colleagues for many a good discussion in the SINTEF CoffeeLab.

The work of RD was performed in support of the US Department of Energy’s Fossil Energy, Oil and Natural Gas Research Program. It was executed by NETL’s Research and Innovation Center, including work performed by Leidos Research Support Team staff under the RSS  
 680 contract 89243318CFE000003. This work was funded by the Department of Energy, National Energy Technology Laboratory, an agency of the United States Government, through a support contract with Leidos Research Support Team (LRST). Neither the United States Government nor any agency thereof, nor any of their employees, nor LRST, nor any of their employees, makes any warranty, expressed or implied, or assumes any legal liability or responsibility for the accuracy, completeness, or usefulness of any information, apparatus, product, or process disclosed, or represents that its use would not infringe privately owned rights. Reference herein to any specific commercial product, process,  
 685 or service by trade name, trademark, manufacturer, or otherwise, does not necessarily constitute or imply its endorsement, recommendation, or favoring by the United States Government or any agency thereof. The views and opinions of authors expressed herein do not necessarily state or reflect those of the United States Government or any agency thereof.

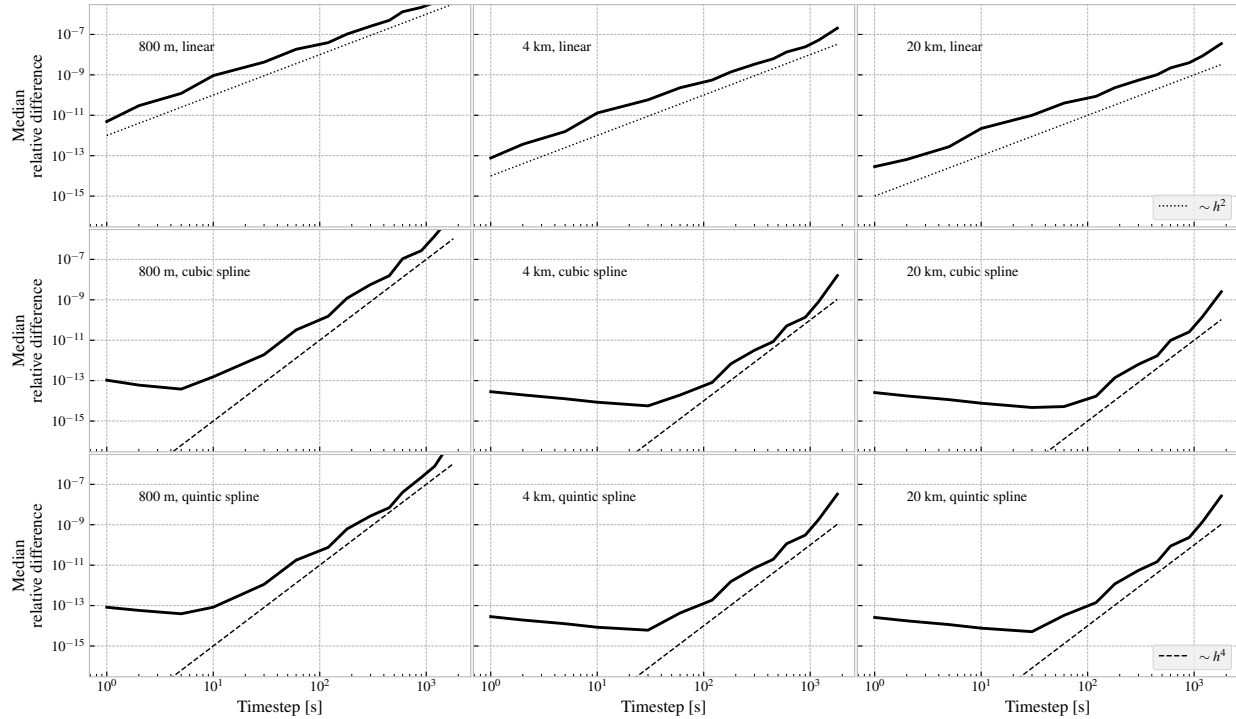


**Figure A3.** Median relative difference (Eq. (A2)) between two 4th-order Runge-Kutta solutions, obtained with different timesteps  $h_i$  and  $h_{i+1}$ , using the list of timesteps in Table A1.

## References

- Ali, S. and Shah, M.: A Lagrangian Particle Dynamics Approach for Crowd Flow Segmentation and Stability Analysis, in: 2007 IEEE  
 690 Conference on Computer Vision and Pattern Recognition, pp. 1–6, <https://doi.org/10.1109/CVPR.2007.382977>, 2007.
- Allshouse, M. R., Ivey, G. N., Lowe, R. J., Jones, N. L., Beegle-Krause, C., Xu, J., and Peacock, T.: Impact of windage on ocean surface  
 Lagrangian coherent structures, *Environmental Fluid Mechanics*, 17, 473–483, 2017.
- Barkan, R., McWilliams, J. C., Molemaker, M. J., Choi, J., Srinivasan, K., Shchepetkin, A. F., and Bracco, A.: Submesoscale dynamics in the  
 northern Gulf of Mexico. Part II: Temperature–salinity relations and cross-shelf transport processes, *Journal of Physical Oceanography*,  
 695 47, 2347–2360, 2017.
- Beron-Vera, F. J., Olascoaga, M. J., and Goni, G. J.: Oceanic mesoscale eddies as revealed by Lagrangian coherent structures, *Geophysical  
 Research Letters*, 35, <https://doi.org/10.1029/2008GL033957>, 2008.
- Beron-Vera, F. J., Olascoaga, M. J., Brown, M. G., Koçak, H., and Rypina, I. I.: Invariant-tori-like Lagrangian coherent structures in geo-  
 physical flows, *Chaos: An Interdisciplinary Journal of Nonlinear Science*, 20, 017 514, 2010.
- 700 Bogacki, P. and Shampine, L. F.: A 3 (2) pair of Runge-Kutta formulas, *Applied Mathematics Letters*, 2, 321–325, 1989.
- Breivik, Ø. and Allen, A. A.: An operational search and rescue model for the Norwegian Sea and the North Sea, *Journal of Marine Systems*,  
 69, 99–113, 2008.
- de Boor, C.: *A practical guide to splines*, Springer-Verlag, New York Berlin Heidelberg, 2001.

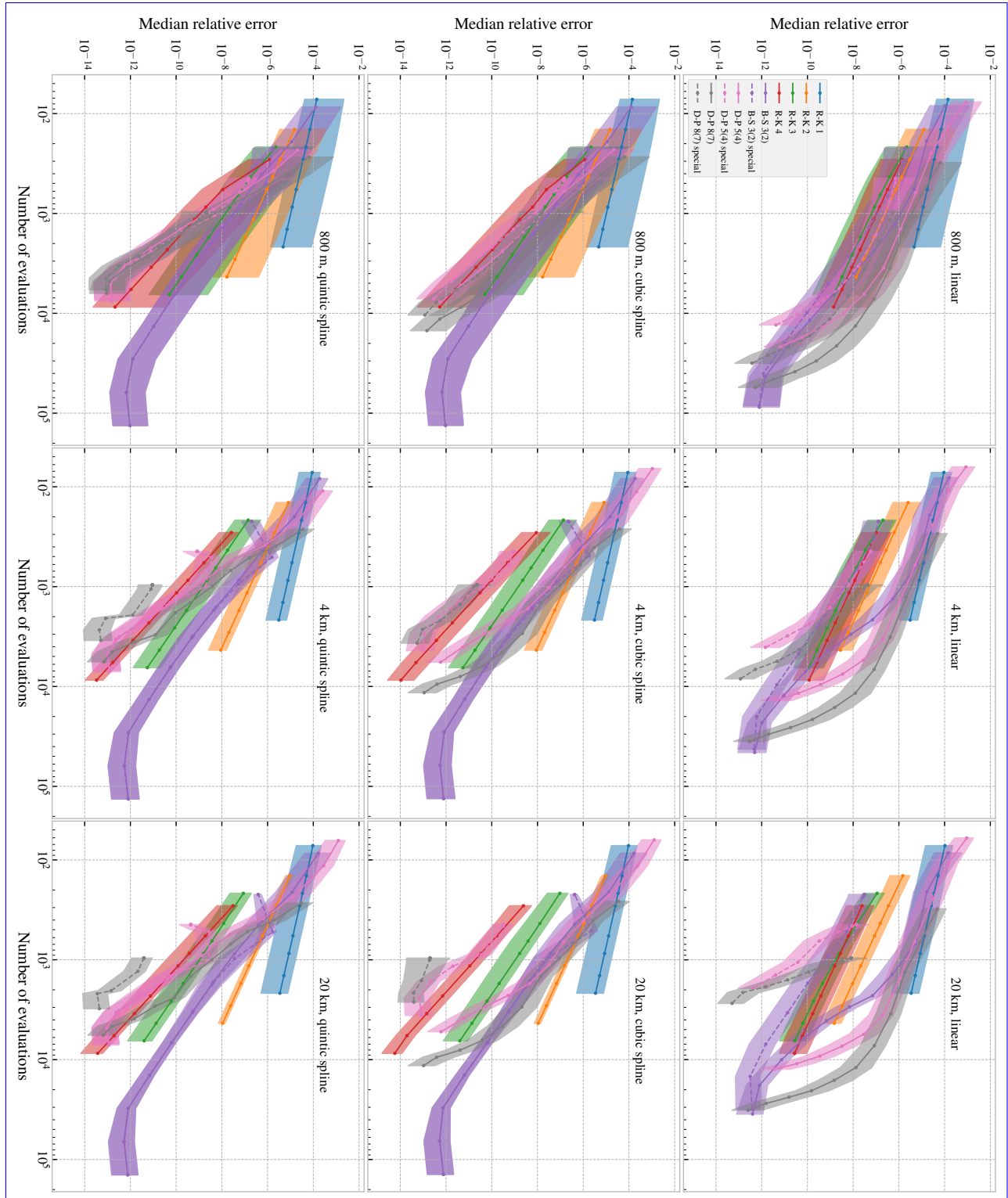
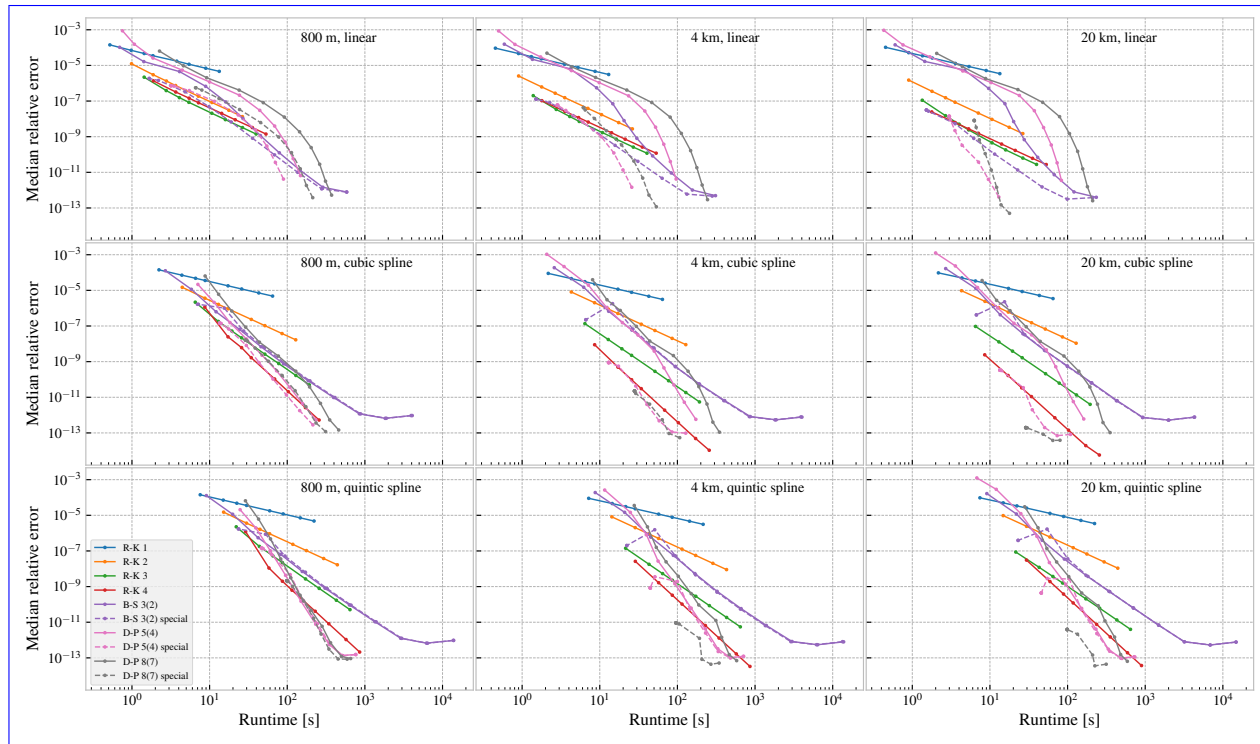


Figure B1. Same as Fig. 5, showing the median relative error, taken over all 10000 trajectories. Additionally, the shaded areas show the range where 90% of the errors fall.





**Figure B2.** Same as Fig. 5, showing the median relative error, taken over all 10000 trajectories, except that the median error is shown as a function of simulation runtime, rather than the number of evaluations of the right-hand side of the ODE.

De Dominicis, M., Pinardi, N., Zodiatis, G., and Lardner, R.: MEDSLIK-II, a Lagrangian marine surface oil spill model for short-term forecasting – Part 1: Theory, *Geoscientific Model Development*, 6, 1851–1869, 2013.

705 Dieci, L. and Lopez, L.: A survey of numerical methods for IVPs of ODEs with discontinuous right-hand side, *Journal of Computational and Applied Mathematics*, 236, 3967 – 3991, <https://doi.org/https://doi.org/10.1016/j.cam.2012.02.011>, <http://www.sciencedirect.com/science/article/pii/S0377042712000684>, 40 years of numerical analysis: “Is the discrete world an approximation of the continuous one or is it the other way around?”, 2012.

710 Dormand, J. and Prince, P.: A family of embedded Runge-Kutta formulae, *Journal of Computational and Applied Mathematics*, 6, 19–26, 1980.

Dormand, J. and Prince, P.: A reconsideration of some embedded Runge-Kutta formulae, *Journal of Computational and Applied Mathematics*, 15, 203–211, [https://doi.org/http://dx.doi.org/10.1016/0377-0427\(86\)90027-0](https://doi.org/http://dx.doi.org/10.1016/0377-0427(86)90027-0), <http://www.sciencedirect.com/science/article/pii/0377042786900270>, 1986.

715 Dugstad, J., Fer, I., LaCasce, J., Sanchez de La Lama, M., and Trodahl, M.: Lateral Heat Transport in the Lofoten Basin: Near-Surface Pathways and Subsurface Exchange, *Journal of Geophysical Research: Oceans*, <https://doi.org/10.1029/2018JC014774>, 2019.

Duran, R., Beron-Vera, F. J., and Olascoaga, M. J.: Extracting quasi-steady Lagrangian transport patterns from the ocean circulation: An application to the Gulf of Mexico, *Scientific reports*, 8, 5218, 2018.

- Enright, W., Jackson, K., Nørsett, S., and Thomsen, P.: Effective solution of discontinuous IVPs using a Runge-Kutta formula pair with interpolants, *Applied Mathematics and Computation*, 27, 313 – 335, [https://doi.org/https://doi.org/10.1016/0096-3003\(88\)90030-6](https://doi.org/https://doi.org/10.1016/0096-3003(88)90030-6), <http://www.sciencedirect.com/science/article/pii/0096300388900306>, 1988.
- Farazmand, M. and Haller, G.: Computing Lagrangian coherent structures from their variational theory, *Chaos: An Interdisciplinary Journal of Nonlinear Science*, 22, 013 128, 2012.
- García-Martínez, R. and Flores-Tovar, H.: Computer modeling of oil spill trajectories with a high accuracy method, *Spill Science & Technology Bulletin*, 5, 323–330, 1999.
- Gladwell, I., Shampine, L., and Thompson, S.: *Solving ODEs with MATLAB*, Cambridge University Press, New York, NY, USA, 2003.
- Gräwe, U.: Implementation of high-order particle-tracking schemes in a water column model, *Ocean Modelling*, 36, 80–89, 2011.
- Griffiths, D. F. and Higham, D. J.: *Numerical methods for ordinary differential equations*, Springer-Verlag, London, 2010.
- Hairer, E. and Wanner, G.: *Solving Ordinary Differential Equations II: Stiff and Differential-Algebraic Problems*, Springer-Verlag Berlin Heidelberg, 1996.
- Hairer, E., Nørsett, S. P., and Wanner, G.: *Solving Ordinary Differential Equations I: Nonstiff Problems*, Springer-Verlag Berlin Heidelberg, 1st edition edn., 1987.
- Hairer, E., Nørsett, S. P., and Wanner, G.: *Solving Ordinary Differential Equations I: Nonstiff Problems*, Springer-Verlag Berlin Heidelberg, 2nd edition edn., 1993.
- Hairer, E., Wanner, G., and Lubich, C.: *Geometric Numerical Integration: Structure-Preserving Algorithms for Ordinary Differential Equations*, Springer-Verlag Berlin Heidelberg, 2006.
- Haller, G.: Lagrangian coherent structures, *Annual Review of Fluid Mechanics*, 47, 137–162, 2015.
- Isaacson, E. and Keller, H. B.: *Analysis of Numerical Methods*, Dover Publications, 1994.
- Kloeden, P. E. and Platen, E.: *Numerical Solution of Stochastic Differential Equations*, Springer-Verlag Berlin Heidelberg, 1992.
- Kress, R.: *Numerical Analysis*, Springer, 1998.
- Lekien, F. and Marsden, J.: Tricubic interpolation in three dimensions, *International Journal for Numerical Methods in Engineering*, 63, 455–471, <https://doi.org/10.1002/nme.1296>, 2005.
- Lévy, M., Resplandy, L., Klein, P., Capet, X., Iovino, D., and Éthé, C.: Grid degradation of submesoscale resolving ocean models: Benefits for offline passive tracer transport, *Ocean Modelling*, 48, 1–9, 2012.
- Maslo, A., de Souza, J. M. A. C., Andrade-Canto, F., and Outerelo, J. R.: Connectivity of deep waters in the Gulf of Mexico, *Journal of Marine Systems*, 203, 103 267, 2020.
- Narváez, D. A., Klinck, J. M., Powell, E. N., Hofmann, E. E., Wilkin, J., and Haidvogel, D. B.: Modeling the dispersal of eastern oyster (*Crassostrea virginica*) larvae in Delaware Bay, *Journal of Marine Research*, 70, 381–409, 2012.
- Nieto, R. and Gimeno, L.: A database of optimal integration times for Lagrangian studies of atmospheric moisture sources and sinks, *Scientific data*, <https://doi.org/10.1038/s41597-019-0068-8>, 2019.
- Nordam, T.: nordam/ODE-integrators-for-Lagrangian-particles 0.9, <https://doi.org/10.5281/zenodo.4041979>, 2020.
- Nordam, T., Brønner, U., Skancke, J., Nepstad, R., Rønningen, P., and Alver, M. O.: Numerical integration and interpolation in marine pollutant transport modelling, in: *Proceedings of the 40th AMOP Technical Seminar*, Calgary, AB, Canada, pp. 586–609, <hdl.handle.net/11250/2653393>, 2017.

- 755 North, E. W., Adams, E. E., Schlag, Z., Sherwood, C. R., He, R., Hyun, K. H., and Socolofsky, S. A.: Simulating Oil Droplet Dispersal From the Deepwater Horizon Spill With a Lagrangian Approach, in: *Monitoring and Modeling the Deepwater Horizon Oil Spill: A Record Breaking Enterprise*, pp. 217–226, 2011.
- Onink, V., Wichmann, D., Delandmeter, P., and van Sebille, E.: The Role of Ekman Currents, Geostrophy, and Stokes Drift in the Accumulation of Floating Microplastic, *Journal of Geophysical Research: Oceans*, 124, 1474–1490, <https://doi.org/10.1029/2018JC014547>,  
760 2019.
- Onu, K., Huhn, F., and Haller, G.: LCS Tool: A computational platform for Lagrangian coherent structures, *Journal of Computational Science*, 7, 26–36, 2015.
- Peng, J. and Dabiri, J. O.: Transport of inertial particles by Lagrangian coherent structures: application to predator–prey interaction in jellyfish feeding, *Journal of Fluid Mechanics*, 623, 75–84, <https://doi.org/10.1017/S0022112008005089>, 2009.
- 765 Povinec, P., Gera, M., Holý, K., Hirose, K., Lujaniené, G., Nakano, M., Plastino, W., Sýkora, I., Bartok, J., and Gažák, M.: Dispersion of Fukushima radionuclides in the global atmosphere and the ocean, *Applied Radiation and Isotopes*, 81, 383–392, <https://doi.org/https://doi.org/10.1016/j.apradiso.2013.03.058>, 6th International Conference on Radionuclide Metrology - Low Level Radioactivity Measurement Techniques, 2013.
- Press, W. H., Teukolsky, S. A., Vetterling, W. T., and Flannery, B. P.: *Numerical recipes 3rd edition: The art of scientific computing*, Cambridge university press, 2007.  
770
- Riuttanen, L., Hulkkonen, M., Dal Maso, M., Junninen, H., and Kulmala, M.: Trajectory analysis of atmospheric transport of fine particles, SO<sub>2</sub>, NO<sub>x</sub> and O<sub>3</sub> to the SMEAR II station in Finland in 1996–2008, *Atmospheric Chemistry and Physics*, <https://doi.org/10.5194/acp-13-2153-2013>, 2013.
- Rivas, D. and Samelson, R. M.: A Numerical Modeling Study of the Upwelling Source Waters along the Oregon Coast during 2005, *Journal of Physical Oceanography*, 41, 88–112, <https://doi.org/10.1175/2010JPO4327.1>, 2011.  
775
- Rye, H., Reed, M., and Ekrol, N.: The ParTrack model for calculation of the spreading and deposition of drilling mud, chemicals and drill cuttings, *Environmental Modelling & Software*, 13, 431–441, 1998.
- Sætre, R.: *The Norwegian Coastal Current: Oceanography and Climate*, Tapir Akademisk Forlag, Trondheim, 2005.
- Serra, M., Sathe, P., Rypina, I., Kirincich, A., Ross, S. D., Lermusiaux, P., Allen, A., Peacock, T., and Haller, G.: Search and rescue at sea  
780 aided by hidden flow structures, 2019.
- Shadden, S. C. and Taylor, C. A.: Characterization of Coherent Structures in the Cardiovascular System, *Annals of Biomedical Engineering*, 36, 1152–1162, <https://doi.org/10.1007/s10439-008-9502-3>, 2008.
- Shadden, S. C., Astorino, M., and Gerbeau, J.-F.: Computational analysis of an aortic valve jet with Lagrangian coherent structures, *Chaos: An Interdisciplinary Journal of Nonlinear Science*, 20, 017 512, <https://doi.org/10.1063/1.3272780>, 2010.
- 785 Siegel, D., Kinlan, B., Gaylord, B., and Gaines, S.: Lagrangian descriptions of marine larval dispersion, *Marine Ecology Progress Series*, 260, 83–96, 2003.
- Sirois, A. and Bottenheim, J. W.: Use of backward trajectories to interpret the 5-year record of PAN and O<sub>3</sub> ambient air concentrations at Kejimikujik National Park, Nova Scotia, *Journal of Geophysical Research: Atmospheres*, 100, 2867–2881, <https://doi.org/10.1029/94JD02951>, <https://agupubs.onlinelibrary.wiley.com/doi/abs/10.1029/94JD02951>, 1995.
- 790 Spivakovskaya, D., Heemink, A. W., and Deleersnijder, E.: Lagrangian modelling of multi-dimensional advection-diffusion with space-varying diffusivities: theory and idealized test cases, *Ocean Dynamics*, 57, 189–203, 2007.

- Van Sebille, E., Scussolini, P., Durgadoo, J. V., Peeters, F. J., Biastoch, A., Weijer, W., Turney, C., Paris, C. B., and Zahn, R.: Ocean currents generate large footprints in marine palaeoclimate proxies, *Nature Communications*, 6, 1–8, 2015.
- 795 van Sebille, E., Griffies, S. M., Abernathey, R., Adams, T. P., Berloff, P., Biastoch, A., Blanke, B., Chassignet, E. P., Cheng, Y., Cotter, C. J., Deleersnijder, E., Döös, K., Drake, H. F., Drijfhout, S., Gary, S. F., Heemink, A. W., Kjellsson, J., Koszalka, I. M., Lange, M., Lique, C., MacGilchrist, G. A., Marsh, R., Mayorga Adame, C. G., McAdam, R., Nencioli, F., Paris, C. B., Piggott, M. D., Polton, J. A., Rühls, S., Shah, S. H., Thomas, M. D., Wang, J., Wolfram, P. J., Zanna, L., and Zika, J. D.: Lagrangian ocean analysis: Fundamentals and practices, *Ocean Modelling*, 121, 49–75, 2018.
- 800 Visser, A. W.: Lagrangian modelling of plankton motion: From deceptively simple random walks to Fokker-Planck and back again, *Journal of Marine Systems*, 70, 287–299, 2008.
- Williams, J.: Bspline-Fortran: Multidimensional B-Spline Interpolation of Data on a Regular Grid, <https://doi.org/10.5281/zenodo.1215290>, 2018.
- Woods, J.: The Lagrangian Ensemble metamodel for simulating plankton ecosystems, *Progress in Oceanography*, 67, 84–159, 2005.
- 805 Yang, Y., He, G.-W., and Wang, L.-P.: Effects of subgrid-scale modeling on Lagrangian statistics in large-eddy simulation, *Journal of Turbulence*, p. N8, 2008.
- Zelenke, B., O'Connor, C., Barker, C., Beegle-Krause, C., and (Eds.), L. E.: General NOAA Operational Modeling Environment (GNOME), Technical Documentation, NOAA Technical Memorandum NOS OR&R 40, NOAA Technical Memorandum NOS OR&R 40, p. 105, <http://response.restoration.noaa.gov/sites/default/files/GNOME{ }Tech{ }Doc.pdf{ }5Cnhttp://response.restoration.noaa.gov/gnome{ }manual>, 2012.